SOILS AND FOUNDATIONS Vol. 48, No. 6, 771–790, Dec. 2008
Japanese Geotechnical Society

SOIL-WATER COUPLED FINITE DEFORMATION ANALYSIS BASED ON A RATE-TYPE EQUATION OF MOTION INCORPORATING THE SYS CAM-CLAY MODEL

Toshihiro Noda[i], Akira Asaoka[i] and Masaki Nakano[i]

ABSTRACT

This paper presents a new method of soil-water coupled finite deformation analysis of saturated soils that considers inertial forces. This method allows changes in the geometric shape of the soil to be taken into account and is capable of dealing with all types of external forces irrespective of whether they are static or dynamic. To be more specific, the paper describes the following points, which differ from the conventional methods: 1) the governing equations for saturated soil including the rate-type equation of motion containing a jerk term of the soil skeleton conforming to ***u-p*** formulation and updated Lagrangian, 2) derivation of a weak form of the rate-type equation of motion and discretization of the finite elements, and 3) use of the implicit time integration method for application of the conventional linear acceleration method (which assumes linear variation of acceleration) to the jerk term. By mounting the elasto-plastic constitutive equation (SYS Cam-clay model), which can cover a wide range of soils and soil conditions, onto the above method of analysis, examples of simulation of dynamic/static triaxial laboratory testing of saturated soil specimens are described. The soil specimens were assumed to be medium dense sand under conditions of small-amplitude cyclic loading, partial drainage, and constant cell pressure. The simulation yielded the following results: (1) In the case of low frequencies, compaction occurs during loading and compression progresses over the entire specimen. (2) In the case of high frequencies, during loading and in the period in which wave propagation continues within the specimen after the end of loading, compaction occurs at the drained end of the specimen, whereas liquefaction occurs in its interior. After this stage, massive compression takes place within the specimen, leading to consolidation (consolidation after liquefaction).

Key words: compaction, (dynamic/static), (finite deformation theory), liquefaction, (soil-water coupled analysis), (SYS Cam-clay model) (**IGC**: E13)

INTRODUCTION

In their past work, the authors and their co-researchers have performed soil-water coupled (quasi-)static finite deformation analyses (Asaoka et al., 1994, 1997; Noda et al., 2005) using the SYS Cam-clay model (Asaoka et al., 1998a, 2000, 2002; Asaoka, 2003) as the constitutive equation, and have succeeded in dealing with all kinds of (quasi-)static soil problems within a single theoretical system, (1) for any required sort of soil from sand through intermediate soils to clay (Asaoka et al., 2002; Asaoka, 2003; Yamada and Nakano, 2007; Nakano et al., 2008), and (2) regardless of whether the problem concerns consolidation deformation or bearing capacity (Noda et al., 2007). By ''a single theoretical system,'' two things are meant. The first meaning is that the SYS Cam-clay model is able to handle the dense multiplicity of really existing soils, from sands through intermediate soils to clays within a single theoretical framework merely by controlling the rate of change per unit amount of elasto-plastic deformation for the three variables of overconsolidation loss, structure decay and induced anisotropy development. Closer details concerning the three evolution rules for overconsolidation, structure and anisotropy can be found in Asaoka et al. (2002) and Asaoka (2003). The second meaning refers to the calculation. Here, ''a single theoretical system'' means that from the basic equation stage of the finite deformation analysis that correctly integrates some different geometrically nonlinear terms which appear when increment form of equilibrium equation arises; this allows not only an analysis of the kind of stable state conditions found with consolidation deformation, in which the increment in the work by external forces is positive, but also a continuous calculation of the kind of processes found, for example, in bearing capacity problems after the loading has peaked, in which there is a switch in state from stable to unstable and hence a negative increment in work by external force. In these two senses, the authors and their colleagues have felt justified in using the name *All Soils All States Geo-Analysis In-*

i) Professor, Department of Civil Engineering, Nagoya University, Japan (noda@civil.nagoya-u.ac.jp).
The manuscript for this paper was received for review on May 19, 2008; approved on October 3, 2008.
Written discussions on this paper should be submitted before July 1, 2009 to the Japanese Geotechnical Society, 4-38-2, Sengoku, Bunkyo-ku, Tokyo 112-0011, Japan. Upon request the closing date may be extended one month.

tegration to describe this analysis method.

The aim of this paper is to present a further application of this ''all-round'' method in the form of a soil-water coupled finite deformation analysis of an inertial force response, demonstrating how it is possible to do away with the existing restriction that limits such problems to (quasi-)static external force states and to tackle instead all kinds of states, static or dynamic. As the incorporation of the SYS Cam-clay model is an absolute precondition for this, it also goes without saying that another aspect of the same aim is to show in effect that this method lives up to its name as an ''*All Soils All States, and effectively All Round, Geo-Analysis Integration*.'' An account of this rate-type equation of motion will be given below, but the purpose for this is not so as to perform a finite deformation analysis as an end in itself, but because it is simply necessary to have a rate-type equation of motion in order for the SYS Cam-clay model to be incorporated into it as a rate-type constitutive equation.

First, the governing equations of the initial-boundary value problems required by this analysis method are presented. At this point, the formulation of the governing equation including the inertial force is given based on conventional two-phase mixture theory, and also as the ''***u-p*** formulation.'' That is, it also has to be hypothesized that the relative acceleration of the fluid phase (pore water) with respect to the solid phase (soil skeleton) is considerably smaller than the acceleration of the solid phase. To make it possible to perform finite deformation analyses based on the updated Lagrangian approach, material time derivative is included following Nishimura (1999) in the equation of motion of the mixture (saturated soil) viewed from the solid phase, in order to give the governing as a ''rate type'' equation of motion having a ''jerk,'' that is to say, possessing a first-order derivative for the acceleration of the soil skeleton. The usual practice up until now for the formulation of dynamic problems in which inertial terms appear, even in studies where a rate-type (or incremental-type) constitutive equation is used, has been to formulate without taking the derivative of the inertial term (e.g., Zienkiewicz and Bettes, 1982; Zienkiewicz and Shiomi, 1984; Oka et al., 1991, 1994; Meroi et al., 1995; Li et al., 2004). In other words, the practice has been to do with a second-degree differential equation for the times of such spatial variables as displacements or spatial coordinates in the soil skeleton, instead of using a rate-type formulation for the equation of motion containing the solid and fluid inertial terms. As a result, in the equation of motion that makes use of weak form or finite element discretization, incremental-type constitutive equations were substituted for the effective stress increment, after dividing up the effective stress at the moment of the calculation one time point earlier than the required one and the effective stress increment up to one time point after it. That is, hardly any account was taken of the geometrical nonlinearity that inevitably appears when a rate-type equation of motion is adopted.

The next part of the paper presents a weak form and a finite element discretization procedure for solving a rate-type equation of motion for a saturated soil involving a third-order derivative for the spatial variable of the soil skeleton spatial coordinates. As an implicit finite time difference method for the solution of ordinary differential equations obtained as a result of discretization, it also introduces a calculation procedure which applies a linear ''acceleration'' method on the assumption of linear variation in the ''jerk'' term (not the acceleration, the third-order derivative term in the spatial coordinates) while simultaneously following the θ method of Wilson et al. (1973).

As the simplest possible example of an analysis performed using the procedures presented, the last part of the paper provides results from a numerical simulation of partially drained dynamic and quasi-static repeated triaxial tests assuming a saturated medium dense sand specimen with a fairly small permeability coefficient. These show that under a low-frequency cyclic loading with no significant influence from acceleration, a compaction behavior occurs in the specimen during loading, while at high frequencies with a considerably greater influence from acceleration the specimen displays liquefaction behavior during loading and approaches an unstable state. After the cyclic loading, however, consolidation occurs in the specimen so that it returns to a stable state. As simple as this analysis example is, it is enough to show that the procedure presented in this paper works ''All Round'' as well as in ''All States.''

INITIAL-BOUNDARY VALUE PROBLEMS OF SATURATED SOILS WITH A RATE-TYPE EQUATION OF MOTION IN THE FINITE DEFORMATION REGIME

In mechanical computations of the initial-boundary value problems of saturated soils, formulation of the governing equations is often based on the solid-fluid two-phase mixture theory, and numerical calculations are made using the finite element method or other methods. In this paper, the two-phase mixture theory is examined based on ***u-p*** formulation, which assumes that the relative acceleration of the fluid phase is sufficiently small with respect to the acceleration of the solid phase. In addition, finite deformation analysis is carried out based on updated Lagrangian, which allows changes in the geometric shape of the soil under analysis to be taken into account. For this purpose, the method of Nishimura (1999) is adopted to allot a rate-type equation of motion to the mixture (saturated soil). In other words, the time derivative of the inertia term is used to allot a rate-type equation of motion that contains a jerk term. In this section, we also present governing equations other than the rate-type equation of motion for solving initial-boundary value problems regarding the mechanical behavior of saturated soils. That is to say, (a) an equation of motion of the mixture (saturated soil) and its rate-type equation, (b) soil skeleton-water coupled equations [continuity equation for expressing the geometric constraints between the fluid phase (pore water) and solid phase (soil skeleton) and the

equation for expressing the average velocity of the pore water], (c) effective stress principle, (d) constitutive equation of the soil skeleton, (e) state equation for pore water, (f) compatibility condition, and (g) boundary conditions are described. The initial conditions, however, are excluded. The formulation of the equations of motion for each phase based on mixture theory follows the method of Full formulation, the details of which are described in APPENDIX 1, according to Nishimura (1999). Moreover, in the formulation of the equations below, it is assumed that the motion of the pore water is isotropic. Also, in order to extend the range of applicability of the equations, the case in which soil particles are assumed to be incompressible while pore water is assumed to be compressible is described.

(a) Rate-type equation of motion for saturated soils based on ***u-p*** formulation

We assume that the relative acceleration $\overset{\backprime}{\boldsymbol{v}}_f - \overset{\backprime}{\boldsymbol{v}}_s$ of the fluid phase with respect to the acceleration of the solid phase $\overset{\backprime}{\boldsymbol{v}}_s$ is considerably small.

$$\overset{\backprime}{\boldsymbol{v}}_s \gg \overset{\backprime}{\boldsymbol{v}}_f - \overset{\backprime}{\boldsymbol{v}}_s \tag{1}$$

Here, the superscript "$\backprime$" on the symbol of a variable indicates the material time derivative viewed from the phase that is denoted by the subscripts (s, solid phase; f, fluid phase) on the same variable. In other words, the term $\overset{\backprime}{\boldsymbol{v}}_s$ in Eq. (1) denotes the material time derivative (acceleration of the solid phase) viewed from the solid phase having a velocity $\boldsymbol{v}_s$, and $\overset{\backprime}{\boldsymbol{v}}_f$ denotes the material time derivative (acceleration of the fluid phase) viewed from the fluid phase having a velocity $\boldsymbol{v}_f$.

In addition, assuming that only interaction forces act between the solid phase (soil) and fluid phase (pore water) and using the sum of the respective equations of motion for the solid and fluid phases [Eq. (A1–9)], we obtain the following equation of motion for saturated soil (mixture).

$$\rho \overset{\backprime}{\boldsymbol{v}}_s = \operatorname{div} \boldsymbol{T} + \rho \boldsymbol{b} \tag{2}$$

Here, $\boldsymbol{T}$ is the Cauchy (total) stress tensor (tension: positive), and $\boldsymbol{b}$ is a constant vector denoting the body force vector per unit mass. In the case of quasi-static problems, the acceleration term on the left-hand side of Eq. (2) disappears. In Eq. (2), ρ is the density of the saturated soil, which can be expressed by Eq. (3) as a function of the densities, ρ^s, ρ^f of the soil particle itself, and the pore water, respectively.

$$\rho = (1-n)\rho^s + n\rho^f \tag{3}$$

In the above equation, n is the porosity, which can be expressed by $n = (\mathrm{v}-1)/\mathrm{v} = \mathrm{e}/(1+\mathrm{e})$ using the specific volume v and the void ratio e.

Next, we derive the rate-type equation of motion for a mixture (saturated soil) in the following manner in order to consider the changes in geometry. Since the constitutive equation for a soil skeleton is an increment-type (rate-type) equation, Eq. (2) is integrated with respect to the volume of the mixture (integrated form), and then its material time derivative viewed from the solid phase is derived to again obtain the local form. For simplification, it is also assumed that only the soil particles are incompressible. This yields the following rate-type equation of motion for the mixture (saturated soil).

$$\rho \overset{\backprime\backprime}{\boldsymbol{v}}_s + \{n\mathrm{D}_s\rho^f + \rho^f(\mathrm{tr}\boldsymbol{D}_s)\}(\overset{\backprime}{\boldsymbol{v}}_s - \boldsymbol{b}) = \operatorname{div} \mathrm{D}_s\boldsymbol{S}_t \tag{4}$$

Since the first term on the left-hand side of this equation is the 2nd derivative of velocity, it is a term that may be referred to as rate of acceleration or jerk. D_s denotes the material time derivative viewed from the solid phase, and $\mathrm{D}_s\boldsymbol{S}_t$ is the nominal stress rate of the solid phase represented by Eq. (5), which conforms to the notations used by Yatomi et al. (1989).

$$\mathrm{D}_s\boldsymbol{S}_t = \mathrm{D}_s\boldsymbol{T} + (\mathrm{tr}\boldsymbol{D}_s)\boldsymbol{T} - \boldsymbol{T}\boldsymbol{L}_s^{\mathrm{T}} \tag{5}$$

Here, $\boldsymbol{L}_s$ is the velocity gradient tensor and $\boldsymbol{D}_s$ is the stretching tensor of the solid phase, which are related as $\boldsymbol{D}_s = 1/2(\boldsymbol{L}_s + \boldsymbol{L}_s^{\mathrm{T}})$.

Since velocity, acceleration, and jerk possess no objectivity, the equations of motion represented by Eqs. (2) and (4) above also possess no objectivity. Therefore, we limit the use of these equations to the inertial systems. In the sections below, rules that do not have objectivity except the above are not used (Nishimura, 1999). Since geometric non-linearity has been taken into account from the stage of the equations of motion, a term corresponding to the density change resulting from the shape change of the mixture appears on the left side of Eq. (4), while an advection term of stress appears on the right side of the same equation.

(b) Soil skeleton–pore water coupled equation (continuity equation for saturated soil and average flow velocity equation for pore water)

(b–1) Continuity equation for saturated soil (geometric constraint conditions for the soil skeleton and pore water)

Applying the mass conservation law to each phase and, for the sake of simplification, assuming here too that only the soil particles are incompressible, the continuity equation for saturated soil is obtained as follows (*see* Eq. (A1–4)):

$$\operatorname{div} \boldsymbol{v}_s + \operatorname{div}\{n(\boldsymbol{v}_f - \boldsymbol{v}_s)\} = -\frac{n}{\rho^f}\mathrm{D}_f\rho^f \tag{6}$$

Here, D_f is the material time derivative viewed from the fluid phase. Because $n(\boldsymbol{v}_f - \boldsymbol{v}_s)$ denotes the average flow velocity of the pore water, it can be understood that Eq. (6) shows, as the geometric constraint for the soil skeleton and pore water in saturated soil, that the temporal volume change rate of the soil skeleton in saturated soil will be the amount of discharge of pore water from and into the saturated soil per unit time.

(b–2) Average flow velocity equation for pore water

In the equation of motion for the fluid phase (pore water), the interaction force between the solid and fluid phases is assumed, as has been suggested by Nishimura (1999) (*see* Eq. (A1–8)). In addition, if we assume that the motion of the fluid phase is isotropic, the average flow velocity of the pore water is obtained as shown below.

$$n(\boldsymbol{v}_f-\boldsymbol{v}_s)=-\frac{k}{\gamma_w}(\mathrm{grad}u-\rho^f\boldsymbol{b})-\overset{\backslash}{\boldsymbol{v}}_s\times\frac{\rho^f k}{\gamma_w} \tag{7}$$

In the above equation, k is the permeability coefficient, g is the acceleration due to gravity (that is, the Euclidian norm of the body force vector $\boldsymbol{b}$ in Eq. (2)), and $\gamma_w=\rho^f g$ is the weight per unit volume of water. The formulation of this equation utilizes the relation denoted by $\rho^f\overset{\backslash}{\boldsymbol{v}}_f=\rho^f\overset{\backslash}{\boldsymbol{v}}_s+\rho^f(\overset{\backslash}{\boldsymbol{v}}_f-\overset{\backslash}{\boldsymbol{v}}_s)\cong\rho^f\overset{\backslash}{\boldsymbol{v}}_s$, which is obtained from the assumption made for Eq. (1). The 2nd term on the right-hand side of Eq. (7) contains the acceleration term of the solid phase. In the case of quasi-static problems, this term will disappear. In such a case, Eq. (7) becomes the usually known Darcy Law.

Noticing the relation $\mathrm{D}_f\rho^f=\mathrm{D}_s\rho^f+\mathrm{grad}\rho^f\cdot(\boldsymbol{v}_f-\boldsymbol{v}_s)$, we can introduce this relation into Eqs. (6) and (7) to obtain following equation (soil skeleton-pore water coupled equation), which connects with the equation of motion for saturated soil (Eq. (4)).

$$-\mathrm{div}\left(\frac{\rho^{f^2}k}{\gamma_w}\overset{\backslash}{\boldsymbol{v}}_s\right)+\rho^f\,\mathrm{div}\boldsymbol{v}_s+\mathrm{div}\left\{-\frac{\rho^f k}{\gamma_w}(\mathrm{grad}u-\rho^f\boldsymbol{b})\right\}+n\mathrm{D}_s\rho^f=0 \tag{8}$$

(c) Principle of effective stress

Following the principle of effective stress, we obtain the equation below

$$\boldsymbol{T}=\boldsymbol{T}'-u\boldsymbol{I}, \tag{9}$$

where $\boldsymbol{T}'$ is the Cauchy effective stress (tension: positive), u is the pore water pressure (compression: positive), and $\boldsymbol{I}$ is the identity tensor.

(d) Constitutive equation for the soil skeleton

In this paper, we apply the SYS Cam-clay model (Asaoka et al., 2002) described in APPENDIX 2 to the constitutive equation for the soil skeleton and obtain the following linear relationship between $\mathring{\boldsymbol{T}}'$ and $\boldsymbol{D}_s$.

$$\mathring{\boldsymbol{T}}'=L[\boldsymbol{D}_s],\quad \mathring{\boldsymbol{T}}'=\mathrm{D}_s\boldsymbol{T}'+\boldsymbol{T}'\boldsymbol{\Omega}_s-\boldsymbol{\Omega}_s\boldsymbol{T}',\quad \boldsymbol{\Omega}_s=\mathrm{D}_s\boldsymbol{R}_s\boldsymbol{R}_s^T \tag{10}$$

where $\mathring{\boldsymbol{T}}'$ is the Cauchy effective stress rate tensor with objectivity. In the calculation example in this paper, the Green-Nagdhi's (1965) Cauchy effective stress rate tensor has been used. $\boldsymbol{\Omega}_s$ is the material spin tensor of the solid phase and $\boldsymbol{R}_s$ is the rotational tensor that is derived from the deformation gradient tensor.

(e) State equation for pore water

The state of the pore water is represented as a function of the pore water pressure by the equation given below.

$$\rho^f=\rho_0\exp\{(u-u_0)/K_f\}, \tag{11}$$

where ρ_0 is the density of the pore water itself under a water pressure of u_0, and K_f is the bulk modulus of the pore water.

(f) Compatibility condition

Although this should be a relation that there is no inconsistency between global and local deformation fields, the definition of the velocity gradient tensor $\boldsymbol{L}_s$ is adopted here.

$$\boldsymbol{L}_s=\frac{\partial\boldsymbol{v}_s}{\partial\boldsymbol{x}} \tag{12}$$

(g) Boundary conditions

In the sub-sections (a) to (f) above, the number of unknowns is equal to the number of equations containing those unknowns. Therefore, the equations can be solved by allotting the boundary conditions. The boundary conditions are described below.

The types of boundary conditions for saturated soil are traction (rate) boundary conditions related to stresses and stress rates, geometrical boundary conditions related to deformation, velocity or acceleration, and hydraulic boundary conditions related to the total head of water and the discharge volume of pore water. These can be written as

$$\Gamma=\Gamma_v+\Gamma_t=\Gamma_q+\Gamma_h, \tag{13}$$

where Γ_v is the geometrical boundary of the saturated soil (mixture), Γ_t is the traction (rate) boundary, Γ_q is the discharge boundary of the pore water, and Γ_h (or Γ_u) is the boundary related to the total head (or pore water pressure). For cases as in this paper, where we consider triaxial tests under constant cell pressures (Asaoka et al., 1994), the traction vector $\boldsymbol{t}$ is given by $\boldsymbol{t}=c\boldsymbol{n}$ (c is a constant and $\boldsymbol{n}$ is the outward normal vector of the boundary), and the rate-type boundary condition for Γ_t becomes.

$$\dot{\boldsymbol{s}}_t da=(\boldsymbol{t}da)^{\cdot}=c(\boldsymbol{n}da)^{\cdot}=c\{(\mathrm{tr}\boldsymbol{D}_s)\boldsymbol{I}-\boldsymbol{L}_s^{\mathrm{T}}\}\boldsymbol{n}da\ \text{on}\ \Gamma_t, \tag{14}$$

where $\dot{\boldsymbol{s}}_t$, in general, is called the nominal traction rate. In other words, when the cell pressure is constant, $\dot{\boldsymbol{s}}_t$ is allotted to the boundary only through the shape variation of the specimen. With respect to the hydraulic boundary conditions, if Γ_q is an undrained boundary, the discharge q per unit area is given below.

$$q=n(\boldsymbol{v}_f-\boldsymbol{v}_s)\cdot\boldsymbol{n}=0 \tag{15}$$

WEAK FORM OF THE RATE-TYPE EQUATION OF MOTION AND FINITE ELEMENT DISCRETIZATION

Weak form of the Rate-type Equation

In order to solve numerically the initial-boundary value problems described in the previous section, we make use of the weak form of the rate-type equation of motion (weak form of Eq. (4)). Through this, the partial differential equations that contain spatial and time variables are converted to ordinary differential equations containing only time variables. To make things simpler, the subscript "s" is removed from the variables that contain it. In addition, the superscript "$\backslash$", which denotes the material time derivative viewed from the solid phase is changed and shown here as the symbol "$\cdot$".

The rate-type equation of motion (Eq. (4)) is integrated with respect to the volume after being taken the inner product with an imaginary vector $\delta\boldsymbol{v}$, which becomes zero at the displacement rate boundary Γ_v shown in Eq. (13)

and also satisfies the compatibility condition (Eq. (12)). Then, using Gauss's divergence theorem, the principle of effective stress (Eq. (9)), and the Green-Naghdi's effective stress rate (Eq. (10)[2]), we obtain the following equation.

$$\int_v \rho\ddot{\boldsymbol{v}}\cdot\delta\boldsymbol{v}dv+\int_v\{\mathring{\boldsymbol{T}}'\cdot\delta\boldsymbol{D}+(\mathrm{tr}\boldsymbol{D})\boldsymbol{T}\cdot\delta\boldsymbol{L}-\boldsymbol{T}\boldsymbol{L}^{\mathrm{T}}\cdot\delta\boldsymbol{L}\}dv$$
$$+\int_v\rho^f\mathrm{tr}\boldsymbol{D}(\dot{\boldsymbol{v}}-\boldsymbol{b})\cdot\delta\boldsymbol{v}dv$$
$$-\int_v\dot{\boldsymbol{u}}\left\{\mathrm{tr}\delta\boldsymbol{D}-\rho^f\frac{n}{K_f}(\dot{\boldsymbol{v}}-\boldsymbol{b})\cdot\delta\boldsymbol{v}\right\}dv$$
$$=\int_a\dot{\boldsymbol{s}}_t\cdot\delta\boldsymbol{v}da-\int_v(\boldsymbol{\Omega}\boldsymbol{T}'-\boldsymbol{T}'\boldsymbol{\Omega})\cdot\delta\boldsymbol{D}dv \tag{16}$$

In the above equation, the subscript v indicates the volume occupied by the saturated soil under consideration, and a is the traction (rate) boundary Γ_t of Eq. (13). The above equation contains nonlinear terms such as ρ, ρ^f, stresses (effective stress and pore pressure), and acceleration $\dot{\boldsymbol{v}}$, which are decided by obtaining the solution to the problem. Therefore, the calculations at each time step need to be iteratively solved until convergence is obtained (Asaoka et al., 1994). For a quasi-static system in which there is no effect of acceleration and the pore water is incompressible (i.e., K_f is infinite), the above equation agrees completely with that of Asaoka et al. (1994, 1997).

Finite Element Discretization (Formulation of Mass Matrix M, Tangent Stiffness Matrix K, etc.)

Finite element discretization of the volume $\boldsymbol{v}$ under calculation is carried out by dividing the elements into volumes denoted by $\boldsymbol{v}^i$ ($i=1, \cdots, NE$, NE: number of element). By considering the arbitrariness of $\delta\boldsymbol{v}$, we obtain the matrix differential equations below.

$$\mathrm{M}^i\frac{d^2}{dt^2}\{\boldsymbol{v}^i\}+\mathrm{K}^i\{\boldsymbol{v}^i\}-(\mathrm{L}^{i\mathrm{T}}+\mathrm{L}_{\mathrm{c}}^{i\mathrm{T}})\dot{u}^i=\{\dot{\boldsymbol{f}}^i\},$$
$$\{\ddot{\boldsymbol{v}}^i\}\equiv\frac{d^2}{dt^2}\{\boldsymbol{v}^i\} \tag{17}$$

Here, M^i is the mass matrix of the saturated soil element i, K^i is the tangent stiffness matrix of the soil skeleton, L^i is the element matrix that converts the (displacement) velocities of the nodes in element i into a volume change rate, $\mathrm{L}_{\mathrm{c}}^i$ is the element matrix for the water compressibility, $\{\boldsymbol{v}^i\}$ is a vector comprised of the velocities of the nodes, $\dot{u}^i$ is the pore pressure rate of element i, and $\{\dot{\boldsymbol{f}}^i\}$ is a vector for the force velocities of the nodes. More specific forms of these are shown in APPENDIX 3. In the calculation in this paper, 4-nodes iso-parametric elements are used.

PHYSICAL MODEL OF THE SOIL SKELETON –PORE WATER COUPLED EQUATION THAT INCLUDES THE EFFECT OF THE INERTIA TERM

Based on Eq. (8), the following equations are derived with regard to the soil skeleton-water coupled system to represent the pore pressure u at the center of each element (Asaoka et al., 1994) by employing an extended physical model by Christian (Christian, 1968) and Tamura (Akai and Tamura, 1978).

$$\frac{k_i}{g}\mathrm{L}^i\frac{d}{dt}\{\boldsymbol{v}^i\}-\mathrm{L}^i\{\boldsymbol{v}^i\}+\sum_{m=1}^{s}\alpha_m^i(u^m-u^i)=\dot{f}_u^i,$$
$$\{\dot{\boldsymbol{v}}^i\}\equiv\frac{d}{dt}\{\boldsymbol{v}^i\} \tag{18}$$

Here, u^i is the pore pressure of element i, and u^m ($m=1, 2, \cdots, s$) is the pore pressure of element m adjacent to element i. k_i is the permeability coefficient of element i. The number of adjacent elements, s, becomes $s=6$ under 3-dimensional conditions and $s=4$ under 2-dimesional plane strain or axisymmetric conditions. In addition, we have

$$\dot{f}_u^i=-\sum_{m=1}^{s}\gamma_w\alpha_m^i(z_{cm}^i-z_c^i)+q^i, \tag{19}$$

where α_m^i ($m=1, 2, \cdots, s$) is a coefficient that is related to the permeability coefficient. The concrete equation for α_m^i is shown in APPENDIX 4 for the more useful case of the permeability coefficient of a non-uniform material. In the formulation of the above equation, the density ρ^f of the pore water is assumed to be that at the center of the element in the case of pore water that exhibits compressibility, as in the above case for pore pressure.

When the height z from a standard plane in the direction of the body vector $\boldsymbol{b}$ is used in Eq. (19), z_c^i is the height of the center of element i being considered, z_{cm}^i ($m=1, 2, \cdots, s$) is the height of the center of an element m adjacent to element i, and q^i is the amount of water flowing into element i per unit time from the outside. Therefore, as described in the example in this paper, if the effect of height or gravity is not considered as in the case of triaxial testing, the first term on the right-hand side of Eq. (19) becomes zero.

SIMULTANEOUS DIFFERENTIAL EQUATION FOR SOLVING THE FINITE DEFORMATION PROBLEM IN THE CASE OF SATURATED SOIL CONTAINING THE INERTIA TERM

By superposing each element in Eqs. (17)[1] and (18)[1] above, we obtain the following simultaneous differential equation, which must be solved to obtain the solution to the initial-boundary value problems of saturated soil.

$$\begin{bmatrix}\mathrm{M}&0\\0&0\end{bmatrix}\frac{d^2}{dt^2}\begin{Bmatrix}\{\boldsymbol{v}\}\\\{u\}\end{Bmatrix}+\begin{bmatrix}0&-(\mathrm{L}^{\mathrm{T}}+\mathrm{L}_{\mathrm{c}}^{\mathrm{T}})\\\mathrm{L}'&0\end{bmatrix}\frac{d}{dt}\begin{Bmatrix}\{\boldsymbol{v}\}\\\{u\}\end{Bmatrix}$$
$$+\begin{bmatrix}\mathrm{K}&0\\-\mathrm{L}&\mathrm{H}\end{bmatrix}\begin{Bmatrix}\{\boldsymbol{v}\}\\\{u\}\end{Bmatrix}=\begin{Bmatrix}\{\dot{\boldsymbol{f}}\}\\\{\dot{f}_u\}\end{Bmatrix}, \tag{20}$$

where

$$\{\boldsymbol{v}\}=\{\boldsymbol{v}_1^{\mathrm{T}}\ \boldsymbol{v}_2^{\mathrm{T}}\cdots\boldsymbol{v}_j^{\mathrm{T}}\cdots\boldsymbol{v}_{(NP-1)}^{\mathrm{T}}\ \boldsymbol{v}_{NP}^{\mathrm{T}}\}^{\mathrm{T}}, \tag{21}$$
$$\{\dot{\boldsymbol{f}}\}=\{\dot{\boldsymbol{f}}_1^{\mathrm{T}}\ \dot{\boldsymbol{f}}_2^{\mathrm{T}}\cdots\dot{\boldsymbol{f}}_j^{\mathrm{T}}\cdots\dot{\boldsymbol{f}}_{(NP-1)}^{\mathrm{T}}\ \dot{\boldsymbol{f}}_{NP}^{\mathrm{T}}\}^{\mathrm{T}}, \tag{22}$$
$$\{u\}=\{u^1\ u^2\cdots u^i\cdots u^{(NE-1)}\ u^{NE}\}^{\mathrm{T}}, \tag{23}$$
$$\{\dot{f}_u\}=\{\dot{f}_u^1\ \dot{f}_u^2\cdots\dot{f}_u^i\cdots\dot{f}_u^{(NE-1)}\ \dot{f}_u^{NE}\}^{\mathrm{T}}, \tag{24}$$

with $\{\boldsymbol{v}\}$ and $\{\dot{\boldsymbol{f}}\}$ being the respective global expressions

of the velocity vector $\boldsymbol{v}_j$ and the load velocity vector $\dot{\boldsymbol{f}}_j$ of node j ($j=1, \cdots, NP$, NP: number of nodes); $\{u\}$ and $\{\dot{f}_u\}$ are the respective global expressions of the pore pressure u^i of element i and the amount of fluid phase $\dot{f}_u^i$ flowing into and out of element i.

$$\mathrm{M}=\sum_{i=1}^{NE}{}'\mathrm{M}^i, \quad \mathrm{K}=\sum_{i=1}^{NE}{}'\mathrm{K}^i \tag{25}$$

$$\mathrm{H}=[\mathrm{H}^{1^{\mathrm{T}}}\ \mathrm{H}^{2^{\mathrm{T}}}\cdots\mathrm{H}^{i^{\mathrm{T}}}\cdots\mathrm{H}^{(NE-1)^{\mathrm{T}}}\ \mathrm{H}^{NE^{\mathrm{T}}}]^{\mathrm{T}} \tag{26}$$

$$\mathrm{L}=[\mathrm{L}^{1^{\mathrm{T}}}\ \mathrm{L}^{2^{\mathrm{T}}}\cdots\mathrm{L}^{i^{\mathrm{T}}}\cdots\mathrm{L}^{(NE-1)^{\mathrm{T}}}\ \mathrm{L}^{NE^{\mathrm{T}}}]^{\mathrm{T}} \tag{27}$$

$$\mathrm{L}'=\frac{1}{g}[k_1\mathrm{L}^{1^{\mathrm{T}}}\ k_2\mathrm{L}^{2^{\mathrm{T}}}\cdots k_i\mathrm{L}^{i^{\mathrm{T}}}\cdots k_{(NE-1)}\mathrm{L}^{(NE-1)^{\mathrm{T}}}\ k_{NE}\mathrm{L}^{NE^{\mathrm{T}}}]^{\mathrm{T}} \tag{28}$$

$$\mathrm{L}_{\mathrm{c}}=[\mathrm{L}_{\mathrm{c}}^{1^{\mathrm{T}}}\ \mathrm{L}_{\mathrm{c}}^{2^{\mathrm{T}}}\cdots\mathrm{L}_{\mathrm{c}}^{i^{\mathrm{T}}}\cdots\mathrm{L}_{\mathrm{c}}^{(NE-1)^{\mathrm{T}}}\ \mathrm{L}_{\mathrm{c}}^{NE^{\mathrm{T}}}]^{\mathrm{T}} \tag{29}$$

In the above equations, M is the global mass matrix, K is the global tangent stiffness matrix of the soil skeleton, L is the global matrix that converts the velocity of the soil skeleton into its volume change, L′ the matrix obtained by the modification of L, and $\mathrm{L_c}$ is the global matrix obtained from $\mathrm{L}_{\mathrm{c}}^i$ ($i=1, \cdots, NE$). H is the global matrix of the coefficient of permeability obtained from H^i ($i=1, \cdots, NE$), which, as shown in APPENDIX 4, is obtained from α_m in Eq. (18)[1]. The term $\Sigma'_{i=1}^{NE}$ indicates the superposed computational operation that takes into account the correspondence to the node numbers of $\{\boldsymbol{v}^i\}$ and $\{\boldsymbol{v}\}$. Also, L (or L′, $\mathrm{L_c}$) and H are matrices that are obtained by taking into account the correspondence to the node numbers of Eqs. (17)[1], (18)[1], and (20), respectively. In the case of a quasi-static problem, if the pore water is treated as being incompressible, Eq. (20) takes the following form.

$$\begin{bmatrix}0 & -\mathrm{L}^{\mathrm{T}}\\ 0 & 0\end{bmatrix}\frac{d}{dt}\begin{Bmatrix}\{\boldsymbol{v}\}\\ \{u\}\end{Bmatrix}+\begin{bmatrix}\mathrm{K} & 0\\ -\mathrm{L} & \mathrm{H}\end{bmatrix}\begin{Bmatrix}\{\boldsymbol{v}\}\\ \{u\}\end{Bmatrix}=\begin{Bmatrix}\{\dot{\boldsymbol{f}}\}\\ \{\dot{f}_u\}\end{Bmatrix} \tag{30}$$

GLOBAL TANGENTIAL STIFFNESS EQUATION

In order to carry out analysis based on the implicit method with due consideration of the effect of the inertia term, we apply the concept of the linear ''acceleration'' method to the ''jerk'' field. Here, we follow the Wilson's θ method (Wilson et al., 1973), which is an extension of the linear acceleration method, to deal with the time differential term in Eq. (20) by difference approximation. That is, we assume that the displacement of the soil skeleton and/or the jerk term $\dddot{\boldsymbol{v}}(t)$, which is a 3rd derivative term of the spatial coordinates, becomes linear within the time interval between $t=t$ to $t=t+\theta\Delta t$ for $\theta\geq 1$.

$$\{\ddot{\boldsymbol{v}}\}|_{t+\tau}=\{\ddot{\boldsymbol{v}}\}|_t+\frac{\tau}{\theta\Delta t}(\{\ddot{\boldsymbol{v}}\}|_{t+\theta\Delta t}-\{\ddot{\boldsymbol{v}}\}|_t) \tag{31}$$

By integrating this equation successively with respect to τ and using $\tau=\theta\Delta t$, we obtain the following three equations for the acceleration vector $\{\ddot{\boldsymbol{v}}\}$, velocity vector $\{\dot{\boldsymbol{v}}\}$, and position vector $\{\boldsymbol{x}\}$ of the nodes.

$$\{\dot{\boldsymbol{v}}(\theta\Delta t)^2\}|_{t+\theta\Delta t}=\{\dot{\boldsymbol{v}}(\theta\Delta t)^2\}|_t+\frac{1}{2}\{\ddot{\boldsymbol{v}}(\theta\Delta t)^3\}|_t+\frac{1}{2}\{\ddot{\boldsymbol{v}}(\theta\Delta t)^3\}|_{t+\theta\Delta t} \tag{32}$$

$$\{\boldsymbol{v}(\theta\Delta t)\}|_{t+\theta\Delta t}=\{\boldsymbol{v}(\theta\Delta t)\}|_t+\{\dot{\boldsymbol{v}}(\theta\Delta t)^2\}|_t+\frac{1}{3}\{\ddot{\boldsymbol{v}}(\theta\Delta t)^3\}|_t+\frac{1}{6}\{\ddot{\boldsymbol{v}}(\theta\Delta t)^3\}|_{t+\theta\Delta t} \tag{33}$$

$$\{\boldsymbol{x}\}|_{t+\theta\Delta t}=\{\boldsymbol{x}\}|_t+\{\boldsymbol{v}(\theta\Delta t)\}|_t+\frac{1}{2}\{\dot{\boldsymbol{v}}(\theta\Delta t)^2\}|_t+\frac{1}{8}\{\ddot{\boldsymbol{v}}(\theta\Delta t)^3\}|_t+\frac{1}{24}\{\ddot{\boldsymbol{v}}(\theta\Delta t)^3\}|_{t+\theta\Delta t} \tag{34}$$

In the above equations, $\{\ddot{\boldsymbol{v}}(\theta\Delta t)^3\}|_{t+\theta\Delta t}$, $\{\dot{\boldsymbol{v}}(\theta\Delta t)^2\}|_{t+\theta\Delta t}$, $\{\boldsymbol{v}(\theta\Delta t)\}|_{t+\theta\Delta t}$, and $\{\boldsymbol{x}\}|_{t+\theta\Delta t}$ represent the jerk vector ($\times(\theta\Delta t)^3$), acceleration vector ($\times(\theta\Delta t)^2$), velocity vector ($\times\theta\Delta t$), and position vector, respectively, of the nodes. If we change the above terms from $\theta\Delta t$ to Δt, they will become the values at time $t=t+\Delta t$.

In addition, by employing the trapezium rule in the implicit method of analysis with respect to pore water, we obtain the following equation, where $\{u\}|_{t+\theta\Delta t}$ is the pore water pressure and $\{\dot{u}\}|_{t+\theta\Delta t}$ is the pore water pressure velocity at time $t=t+\theta\Delta t$.

$$\{u\}|_{t+\theta\Delta t}=\{u\}|_t+\frac{1}{2}(\{\dot{u}\}|_{t+\theta\Delta t}+\{\dot{u}\}|_t)(\theta\Delta t) \tag{35}$$

Considering Eq. (20) to be valid at time $t=t+\theta\Delta t$ and substituting this equation in Eqs. (32) and (33), the simultaneous 1st degree equation that needs to be solved finally for time $t=t+\theta\Delta t$ is

$$\begin{bmatrix}\dfrac{1}{(\theta\Delta t)^2}\mathrm{M}+\dfrac{1}{6}\mathrm{K} & -2(\mathrm{L}^{\mathrm{T}}+\mathrm{L}_{\mathrm{c}}^{\mathrm{T}})\\ -\mathrm{L}_{\theta 1} & \mathrm{H}\times\theta\Delta t\end{bmatrix}\begin{Bmatrix}\{\ddot{\boldsymbol{v}}(\theta\Delta t)^3\}|_{t+\theta\Delta t}\\ \{u\}|_{t+\theta\Delta t}\end{Bmatrix}$$

$$=\begin{Bmatrix}\{\dot{\boldsymbol{f}}(\theta\Delta t)\}|_{t+\theta\Delta t}-\mathrm{K}\left[\{\boldsymbol{v}(\theta\Delta t)\}|_t+\{\dot{\boldsymbol{v}}(\theta\Delta t)^2\}|_t+\dfrac{1}{3}\{\ddot{\boldsymbol{v}}(\theta\Delta t)^3\}|_t\right]-2(\mathrm{L}^{\mathrm{T}}+\mathrm{L}_{\mathrm{c}}^{\mathrm{T}})\left[\{u\}|_t+\dfrac{1}{2}\{\dot{u}(\theta\Delta t)\}|_t\right]\\ \{\dot{f}_u(\theta\Delta t)\}|_{t+\theta\Delta t}+\mathrm{L}\{\boldsymbol{v}(\theta\Delta t)\}|_t+\mathrm{L}_{\theta 2}\{\dot{\boldsymbol{v}}(\theta\Delta t)^2\}|_t+\mathrm{L}_{\theta 3}\{\ddot{\boldsymbol{v}}(\theta\Delta t)^3\}|_t\end{Bmatrix} \tag{36}$$

where

$$L_{\theta n} = [\gamma^1_{\theta n} L^{1^T} \ \gamma^2_{\theta n} L^{2^T} \cdots \gamma^i_{\theta n} L^{i^T} \cdots \gamma^{(NE-1)}_{\theta n} L^{(NE-1)^T} \ \gamma^{NE}_{\theta n} L^{NE^T}]^T \quad (n = 1, 2, 3), \tag{37}$$

$$\gamma^i_{\theta 1} = \frac{1}{6} - \frac{1}{2\theta \Delta t} \frac{\rho^f k_i}{\gamma_w}, \quad \gamma^i_{\theta 2} = 1 - \frac{1}{\theta \Delta t} \frac{\rho^f k_i}{\gamma_w}, \quad \gamma^i_{\theta 3} = \frac{1}{6}\left(2 - \frac{3}{\theta \Delta t} \frac{\rho^f k_i}{\gamma_w}\right), \tag{38}$$

and θ is the parameter employed in the Wilson's θ method. M, K, $\{\dot{f}(\theta \Delta t)\}|_{t+\theta\Delta t}$, and $\{\dot{f}_u(\theta \Delta t)\}|_{t+\theta\Delta t}$ are renewed by repeating the computation within the time interval steps between $t = t$ and $t = t + \theta \Delta t$. In the calculation example in this paper, θ was set to 1.4 as used in the original Wilson's θ method. We were unable to solve Eq. (36) if $\gamma^i_{\theta 1}$ was negative when k_i and Δt were chosen.

INTRODUCTION OF THE CONSTRAINT CONDITIONS

In this paper, computations are carried out taking the load-controlled triaxial test as an example. Since the pedestal used for triaxial testing is rigid and rough enough to exert sufficient friction, it imparts a constraint to the soil skeleton at the contact surface of the saturated soil. In the case of constraint conditions being inflicted upon deformation of the soil skeleton, the computations are carried out based on the Lagrange multiplier method similar to that described by Asaoka et al. (1998b). In this section, only the ordinary differential equation that needs to be solved in such a case is shown.

Assuming that the constraints are imparted by the position vector $\boldsymbol{x}$, we obtain the following equation by time derivative of the vector viewed from the soil skeleton.

$$C\{v\} = \{0\} \tag{39}$$

Here, C is the matrix imparting the constraint conditions. Since discretization of the weak form of the equation of motion into finite elements is subjected to the constraints $C\{\delta v\} = \{0\}$, the ordinary differential equation that needs to be solved finally is obtained through the Lagrange multiplier method and becomes

$$\begin{bmatrix} M & 0 & 0 \\ 0 & 0 & 0 \\ 0 & 0 & 0 \end{bmatrix} \frac{d^2}{dt^2} \begin{Bmatrix} \{v\} \\ \{u\} \\ \{\lambda\} \end{Bmatrix} + \begin{bmatrix} 0 & -(L^T + L_c^T) & 0 \\ L' & 0 & 0 \\ 0 & 0 & 0 \end{bmatrix} \frac{d}{dt} \begin{Bmatrix} \{v\} \\ \{u\} \\ \{\lambda\} \end{Bmatrix} + \begin{bmatrix} K & 0 & -C^T \\ -L & H & 0 \\ -C & 0 & 0 \end{bmatrix} \begin{Bmatrix} \{v\} \\ \{u\} \\ \{\lambda\} \end{Bmatrix} = \begin{Bmatrix} \{\dot{f}\} \\ \{\dot{f}_u\} \\ \{0\} \end{Bmatrix}, \tag{40}$$

where $\{\lambda\} = \{\lambda_1, \lambda_2, \cdots, \lambda_k, \cdots, \lambda_{(NC-1)}, \lambda_{NC}\}^T$ and $\{\lambda\}$ indicates the vector consisting of the Lagrange multiplier λ_k ($k = 1, \cdots, NC$, NC: number of constraints) pertaining to the kth constraint. Additionally, in regard to this equation and similar to the manner mentioned above, the simultaneous equation of, as shown in Eq. (36), that must be solved can be obtained if difference approximation is applied.

ACCELERATION, VELOCITY, AND POSITION VECTORS AND RENEWAL OF STATE QUANTITIES

In this chapter, we describe the acceleration, velocity, and position vectors and renewal of state quantities. Different equations (formulae) are required for time $t = t + \theta \Delta t$ and $t = t + \Delta t$ as discussed below.

Quantities at Time $t = t + \theta \Delta t$

The acceleration, velocity, and position vectors are determined from Eqs. (32) to (34), respectively, using the solution $\{\ddot{v}(\theta \Delta t)\}|_{t+\theta\Delta t}$ to the global tangent stiffness equation (Eq. (36)). With respect to the stress and other state quantities, if we represent these state quantities (tensor, vector, and scalar quantities) by A and their velocities by $\dot{A}$, the velocity $\dot{A}|_{t+\theta\Delta t}$ of the state quantity at time $t = t + \theta \Delta t$ can be determined from $\{v(\theta \Delta t)\}|_{t+\theta\Delta t}$ obtained above from Eq. (33). Therefore, the state quantity $A|_{t+\theta\Delta t}$ can be determined from the quantities at time $t = t$ according to Eq. (41) below. The pore water pressure, however, is excluded because the water pressure $\{u\}|_{t+\theta\Delta t}$ is decided by the solution to Eq. (36).

$$A|_{t+\theta\Delta t} = A|_t + \frac{1}{2}(\dot{A}|_{t+\theta\Delta t} + \dot{A}|_t)(\theta \Delta t) \tag{41}$$

Quantities at Time $t = t + \Delta t$

The acceleration, velocity, and position vectors at time $t = t + \Delta t$ are computed from the terms $\{\ddot{v}(\theta \Delta t)^3\}|_{t+\theta\Delta t}$ at time $t = t + \theta \Delta t$ and $\{\dot{v}(\theta \Delta t)^2\}|_t$, $\{v(\theta \Delta t)\}|_t$, and $\{x\}|_t$ at time $t = t$ in the equations obtained by making $\tau = \Delta t$ during derivation of Eqs. (32) to (34). In addition, the state quantities $A|_{t+\Delta t}$ at time $t = t + \Delta t$ together with their velocities $\dot{A}|_{t+\Delta t}$ are obtained from the quantities at time $t = t$ and at time $t = t + \theta \Delta t$ using the equations given below.

$$\dot{A}|_{t+\Delta t}(\theta \Delta t) = 2(A|_{t+\theta\Delta t} - A|_t) - \dot{A}|_t(\theta \Delta t) \tag{42}$$

$$A|_{t+\Delta t} = A|_t + \frac{1}{2\theta}\{\dot{A}|_{t+\Delta t}(\theta \Delta t) + \dot{A}|_t(\theta \Delta t)\} \tag{43}$$

OTHER MATTERS

In these computations, during the first stage where the time is incremented from $t = t$ to $t = t + \theta \Delta t$, the acceleration, velocity, position, and various state quantities at time $t = t + \theta \Delta t$ are forecast using explicit formulae (Eulerian approximation).

In addition, judgment of convergence is carried out at

each integration point (each Gauss point) of each element using the relative error derived from the equivalent stress. Update to the next time step is performed if the relative errors at all integration points are sufficiently small (Asaoka et al., 1994).

SIMULATION OF PARTIALLY DRAINED DYNAMIC AND QUASI-STATIC REPEATED TRIAXIAL TESTS OF SATURATED SOIL UNDER A CONSTANT CONFINED PRESSURE

As an example of the computational method described above, we discuss in this chapter simulation of partially drained dynamic and quasi-static repeated triaxial laboratory tests under a constant lateral confined pressure when the cyclic load applied is very small in amplitude. The test specimen is assumed to be saturated sand with a somewhat small permeability coefficient. The effect of gravity is ignored, and the pore water is assumed to be incompressible. That is, $\boldsymbol{b}=\boldsymbol{0}$ in Eq. (2), and in Eq. (11), $\rho^f=\rho_0$ and $K_f=\infty$. In this computational example, liquefaction, the consolidation that occurs after the liquefaction and compaction are simulated systematically.

Calculation Conditions

Figure 1 shows the finite element mesh and boundary conditions used in the computation. For the sake of simplicity, the specimen was assumed to be cylindrical, and the loading conditions were assumed to be axisymmetric and up-down symmetric. This enables the calculations to be carried out with a quarter section of the cylindrical specimen. At the upper boundary of the specimen, the effect of the rigid and rough pedestal was represented by allotting constraint conditions (invariable length and angle) between the nodes (Asaoka et al., 1998b). Treatment was also carried out in order to increase the freedom of movement at the corner (Asaoka et al., 1994). The load was a point load applied at the center of the pedestal at the upper boundary of the specimen (i.e., the node at the left-hand edge of Fig. 1) under constant lateral pressure. After a vertical stress equivalent to amplitude of 40 kPa was applied 20 times using a sine wave loading pattern, the specimen was allowed to stand until it reached the same stress condition as the initial isotropic stress condition. Two cases of frequencies of the cyclic load were considered, a (i) low (period = 100 s) and (ii) high frequency (period = 0.01 s). The hydraulic boundary conditions were assumed to be partial draining with the upper boundary being the drained condition. All other parts were considered to be undrained. Tables 1 and 2 show the assumed material constants of the saturated soil and the initial conditions of the test specimen. Among the material constants allotted, the elasto-plastic parameters and the evolutional parameters were those of a sand-like material with rapid decay of structure and mild loss of overconsolidation, but the permeability coefficient was set at 10^{-5} cm/s assuming a soil with a large fraction of fine particles. In the results of the calculations below, the apparent behavior under axial displacement-controlled monotonic loading at a rate of 0.05 cm/s and undrained condition is first described in order to illustrate the characteristics of the test specimen assumed here.

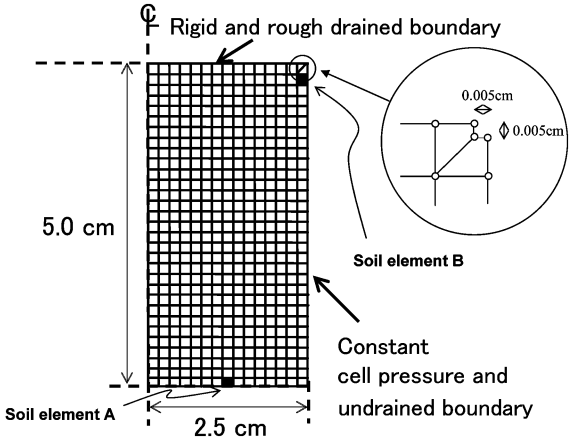

Fig. 1. Finite element mesh and boundary conditions

Table 1. Material constants in the "sand"

Elasto-plastic parameters	
Compression index $\tilde{\lambda}$	0.05
Swelling index $\tilde{\kappa}$	0.012
Critical state constant M	1.0
Specific volume at $q=0$ and $p'=98.1$ kPa on NCL N	1.98
Poisson's ratio ν	0.3
Evolution rule parameters	
Degradation index of structure a ($b=c=1.0$)	2.2
Degradation index of overconsolidation m	0.06
Evolution index of rotational hardening b_r	3.5
Limit of rotational hardening m_b	0.7
Permeability k (cm/s)	1.0×10^{-5}

Table 2. Initial conditions in the specimen

Mean effective stress p'_0 (kPa)	294.3
Specific volume v_0	1.94
Degree of structure $1/R_0^*$	5.0
Overconsolidation ratio $1/R_0$	3.0
Degree of anisotropy $\xi_0=\sqrt{3/2\beta_0\cdot\beta_0}$	0.0

Results of the Calculations

(a) Apparent behavior under monotonic loading with axial displacement control

Figure 2 shows the apparent behavior of the test specimen under monotonic loading. Apparent behavior here means the specimen behavior when viewed as a single element. In the case of the axial displacement rate used, the excess water pressure produced in the test specimen is almost uniform. In the stress calculations, the compensations to the cross section were performed assuming the specimen always remains cylindrical. p' is the mean effective stress and q is the deviator stress, which are denoted by $p'=-\mathrm{tr}\boldsymbol{T}'/3$, $q=\sqrt{3/2\boldsymbol{S}\cdot\boldsymbol{S}}$ ($\boldsymbol{S}=\boldsymbol{T}'+p'\boldsymbol{I}$). It can be seen from the figure that the test specimen exhibits

softening under low stress ratios at first, followed by hardening behavior under high stress ratios. Such a behavior is typical of medium dense sand.

(b) Apparent behavior of the test specimen (liquefaction-induced settlement)

Figures 3 and 4 show the apparent behavior of the test specimen under vertical cyclic loads of low and high frequencies respectively. Since the upper boundary is in a state of drained condition, the excess pore water pressure was taken as zero at this boundary. In these figures and those hereafter, the solid lines (a to b) indicate the behavior during load application, and the broken lines (b to c) indicate the behavior after load application has ended. In the case of low frequency loading (Fig. 3), the specimen exhibits the so-called compaction behavior, where compression begins in the initial stages of load application and ceases once load application ends. In contrast, in the case of high frequency loading (Fig. 4), the specimen behavior is rather similar to undrained behavior, and the axial strain ε_a begins to alternate widely between the compression and tension sides after the 14th cycle. After load application has ended, large consolidation settlement has occurred.

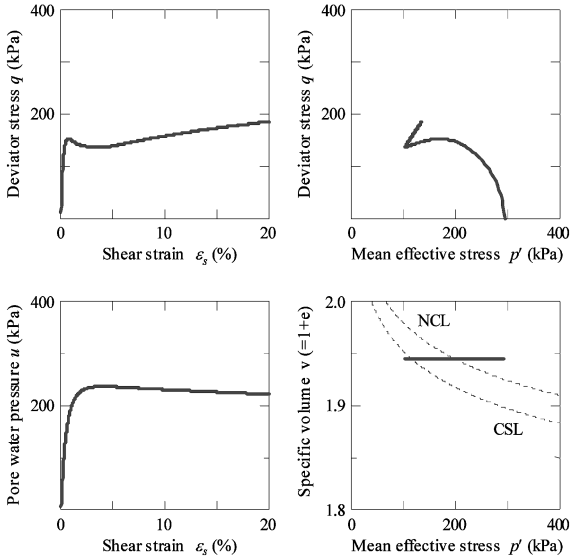

Fig. 2. Medium dense sand-like behavior under undrained monotonic loading

(c) Distributions within the test specimen

Figures 5 to 8 show the temporal distributions of the degree of structure $1/R^*$, overconsolidation ratio $1/R$, specific volume change Δv, and shear strain ε_s in the case of low frequency loading. At the drained boundary, the degree of structure and overconsolidation ratio accumulated somewhat during load application, and together with the appearance of shear strain, compression (consolidation) has occurred locally. Since there is almost no occurrence of excess pore water pressure u_e, there is almost no change in the distributions after load applica-

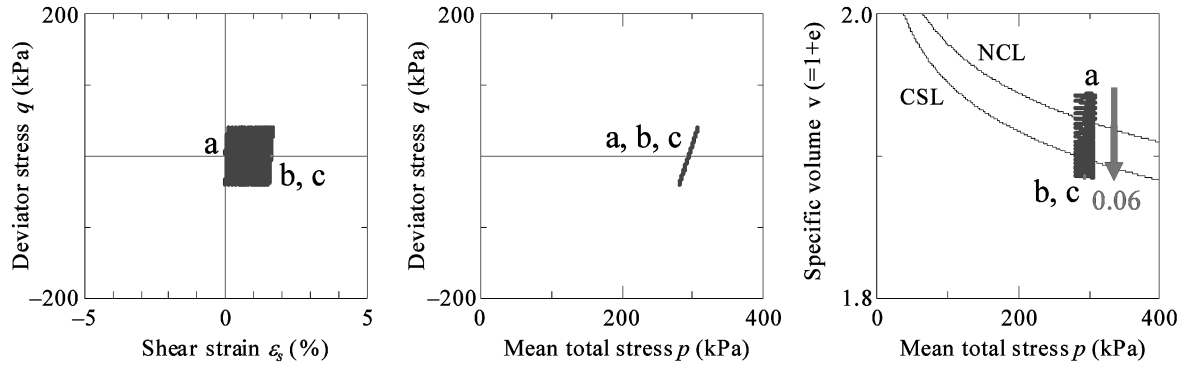

Fig. 3. Compaction behavior (Periods: 100 sec. Number of cycles: 20. $\Delta q = 40$ kPa)

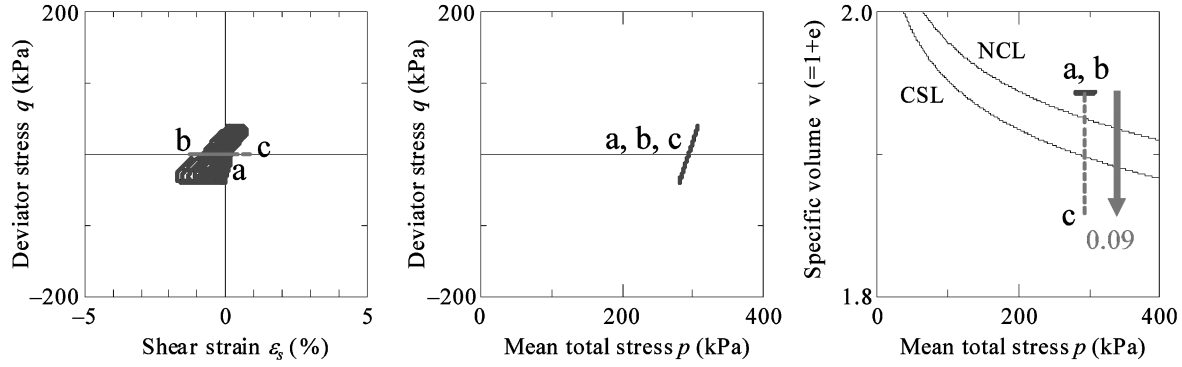

Fig. 4. Liquefaction-induced behavior (Periods: 0.01 sec. Number of cycles: 20. $\Delta q = 40$ kPa)

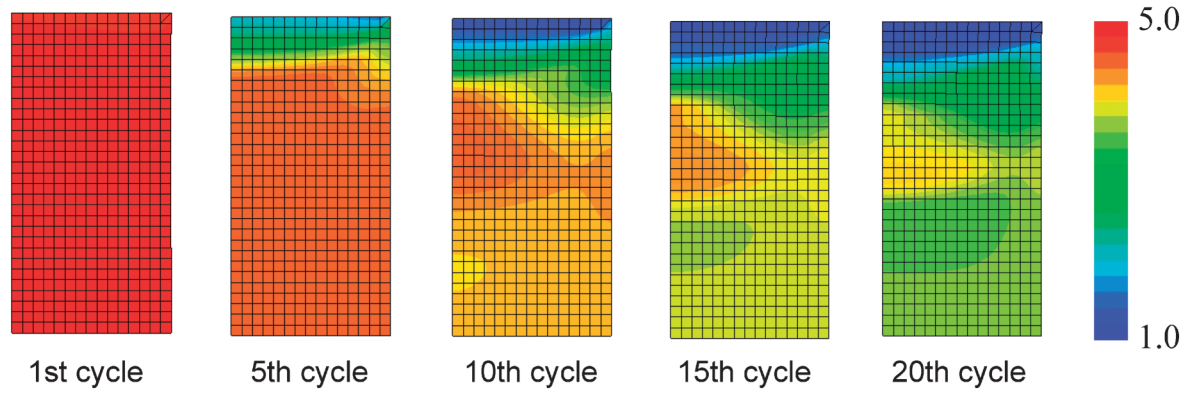

Fig. 5. Distributions of structure, $1/R^*$ with elapsed time (Periods: 100 sec)

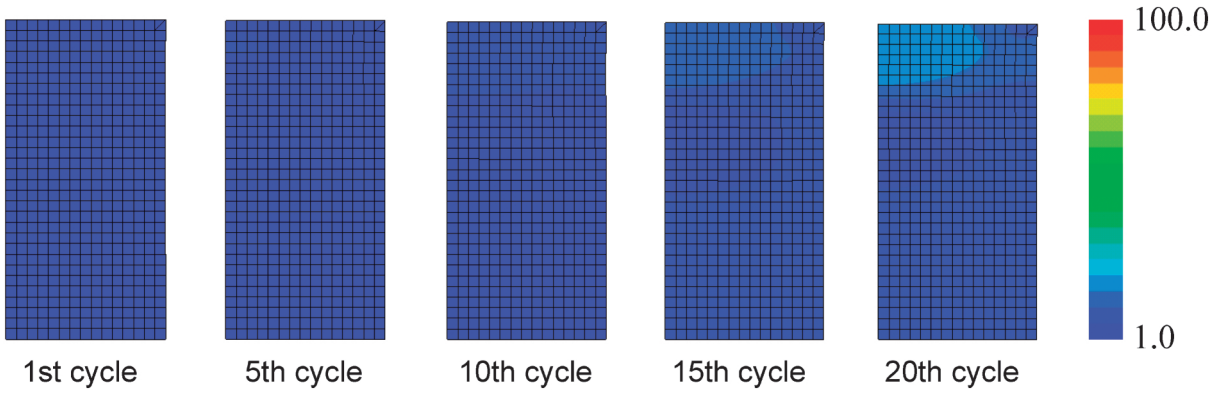

Fig. 6. Distributions of OCR, $1/R$ with elapsed time (Periods: 100 sec)

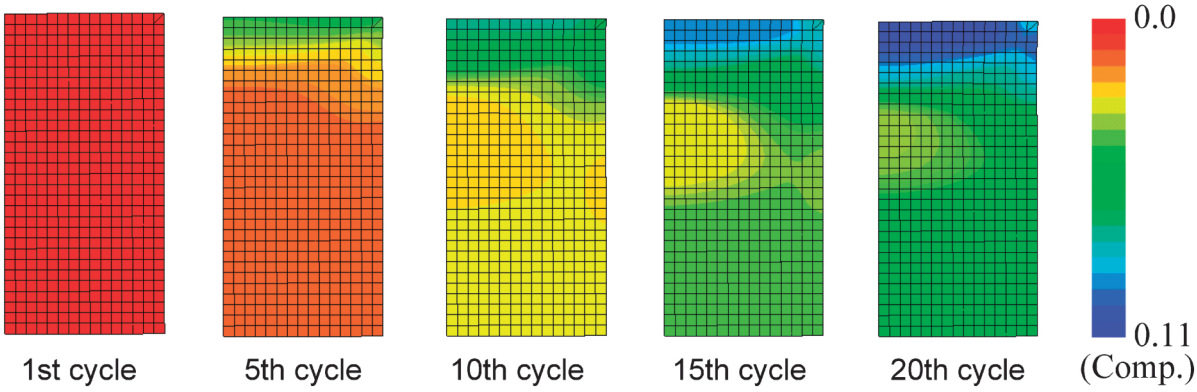

Fig. 7. Distributions of specific volume change, Δv with elapsed time (Periods: 100 sec)

tion has ended.

Figures 9 to 13 show the temporal distributions of $1/R^*$, $1/R$, Δv, ε_s, and u_e in the case of high frequency loading. Each figure shows the distributions of these parameters 0.01, 0.1, 1.0, and 10 sec after the end of load application and those at the end of consolidation. During load application, compaction occurred only near the drained boundary. However, even in the vicinity of the center of the specimen far away from the drained boundary, there was decay of structure, the overconsolidation ratio increased gradually and accumulated to a great extent, and the excess pore water pressure increased to a level approaching the constraint pressure (294 kPa). In addition, shear strain has been produced in the form of a stripe pattern covering the entire test specimen. Even if the load is maintained constant immediately after the application of cyclic load has ended, residual wave propagation within the specimen results in the soil element being subjected to repeated loading/unloading without any pore water migration, as will be described later. This produces a further increase in the excess pore water pressure, and the overconsolidation ratio increases. After this

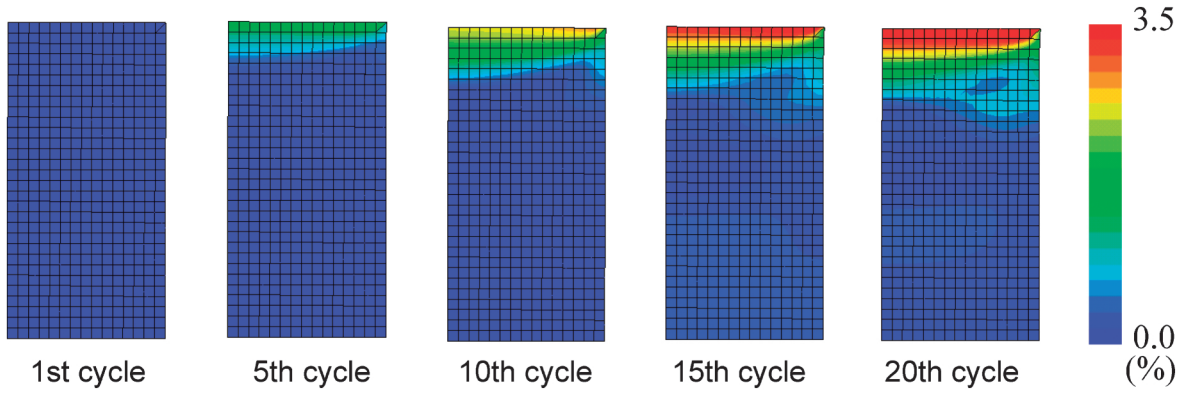

Fig. 8. Distributions of shear strain, ε_s with elapsed time (Periods: 100 sec)

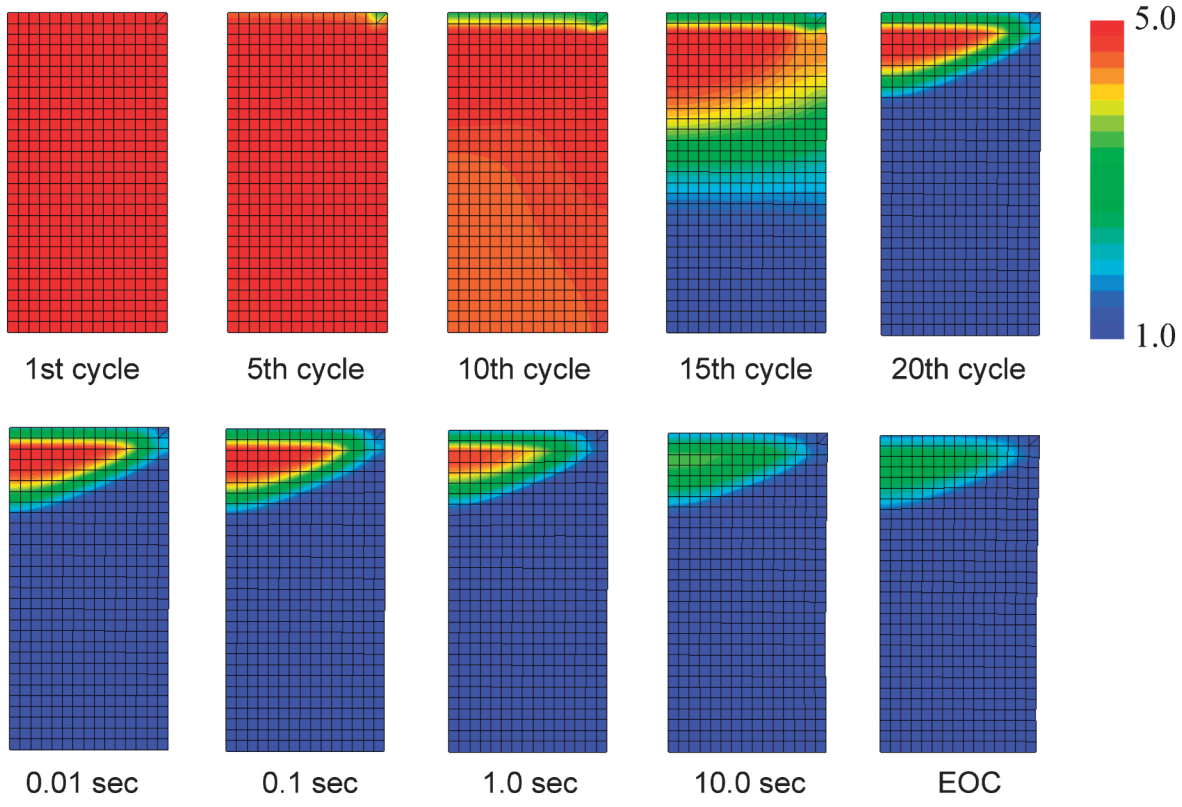

Fig. 9. Distributions of structure, $1/R^*$ with elapsed time (Periods: 0.01 sec)

stage, (i.e., 1.0 sec after load application has ended), the overconsolidation ratio decreases rapidly along with the progress of drainage, and massive compression occurs. In addition, the appearance of shear strain advances at the center and boundaries of the specimen.

(d) Behavior of the soil elements

The behaviors of soil elements A and B under low frequency loading are shown in Figs. 14 and 15, while those under high frequency loading are shown in Figs. 16 and 17. In the case of low frequency loading (Figs. 14 and 15), both elements exhibit compaction during load application, without any significant decrease in p'. In contrast, in the case of high frequency loading (Figs. 16 and 17), the stress acting on deeply located element A approaches the origin with increasing q/p' during load application, and the element exhibits liquefaction behavior. Load application is accompanied by rapid decay of structure while the overconsolidation ratio increases. During the period in which wave propagation continues after the end of cyclic loading (b to b′), the overconsolidation ratio continues to accumulate. Subsequently, consolidation occurs along with relaxation of overconsolidation (b′ to c), and massive compression occurs (consolidation after liquefaction). In contrast to element A, massive compression (compaction) occurs in element B close to the drained boundary along with the slight decrease in p' and increase in q/p' during load application. Compared with element A, the decay of structure in element B is small,

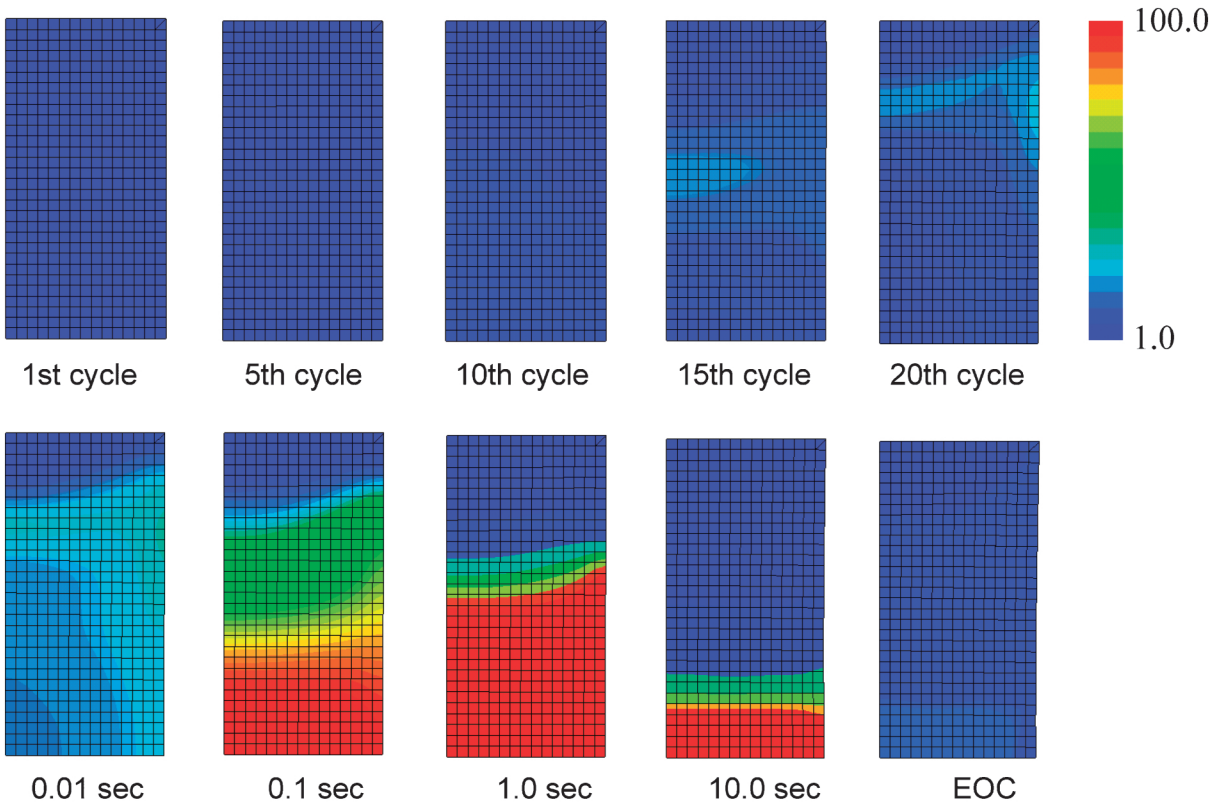

Fig. 10. Distributions of OCR, $1/R$ with elapsed time (Periods: 0.01 sec) (Values exceeding 100 are shown as 100, Max. 1977.5)

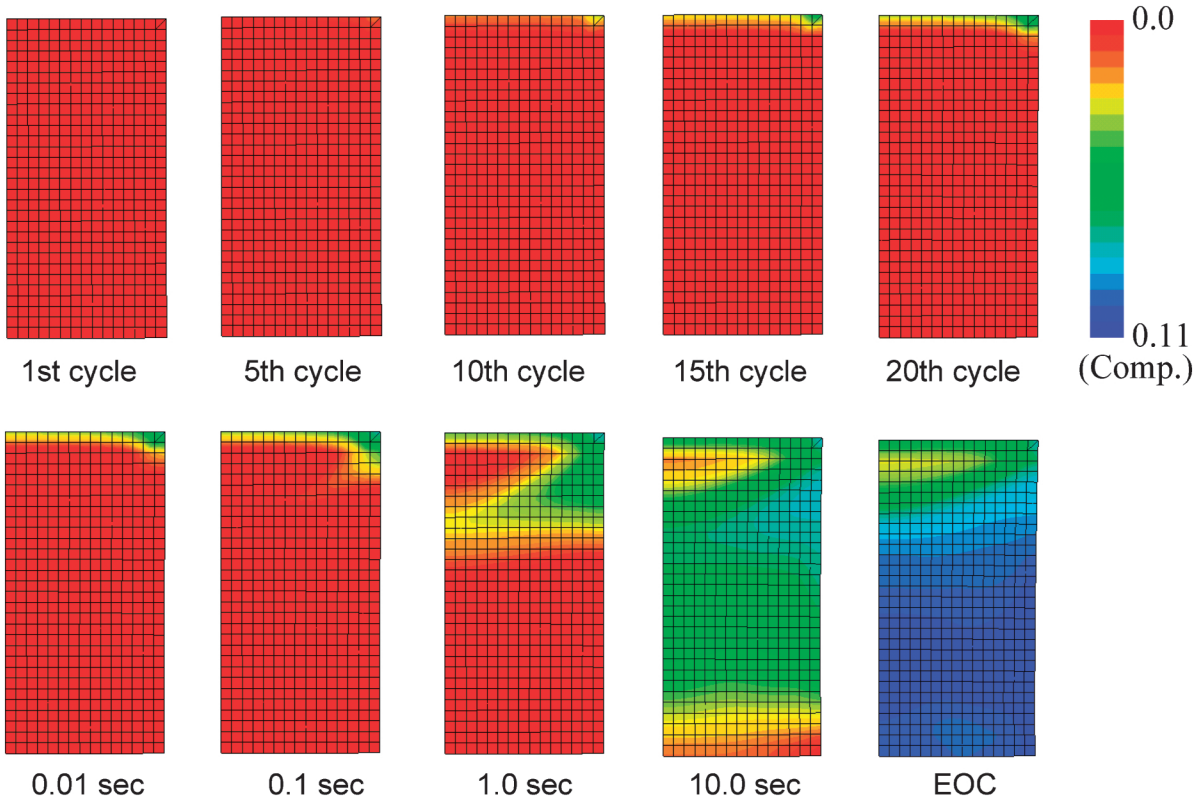

Fig. 11. Distributions of specific volume change, Δv with elapsed time (Periods: 0.01 sec)

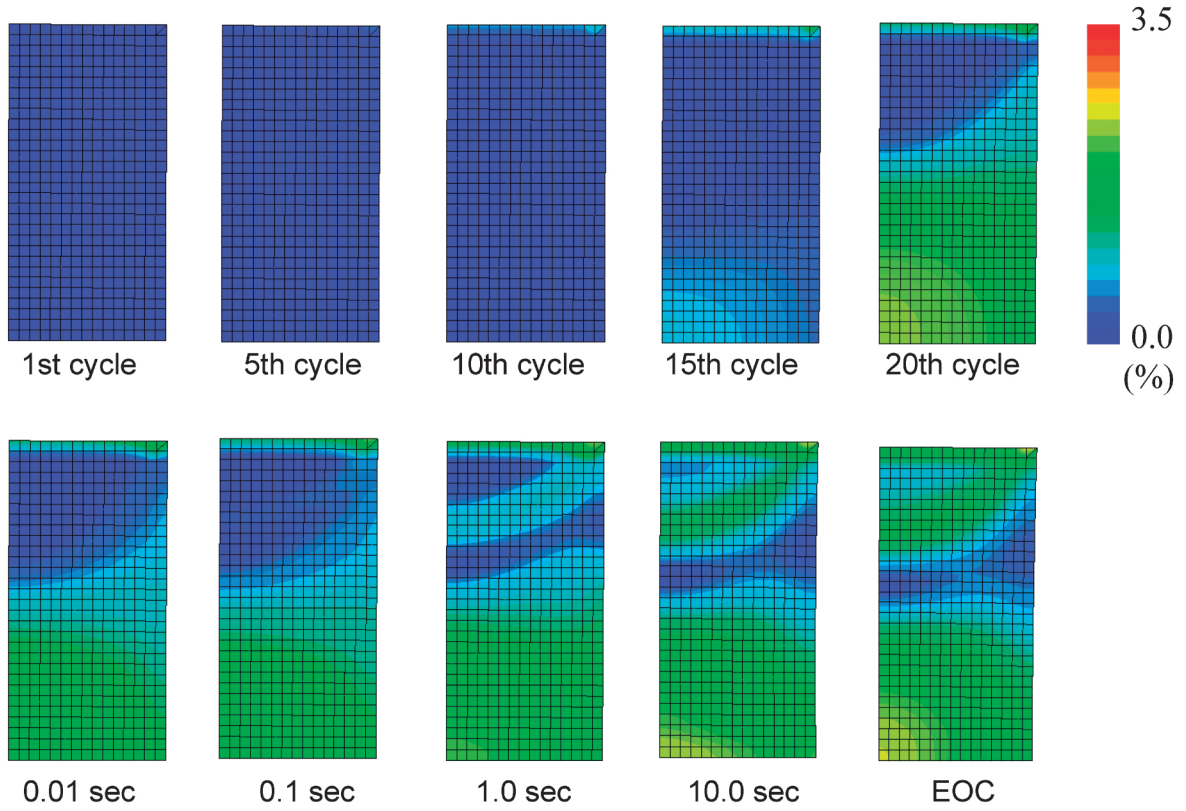

Fig. 12. Distributions of shear strain, ε_s with elapsed time (Periods: 0.01 sec)

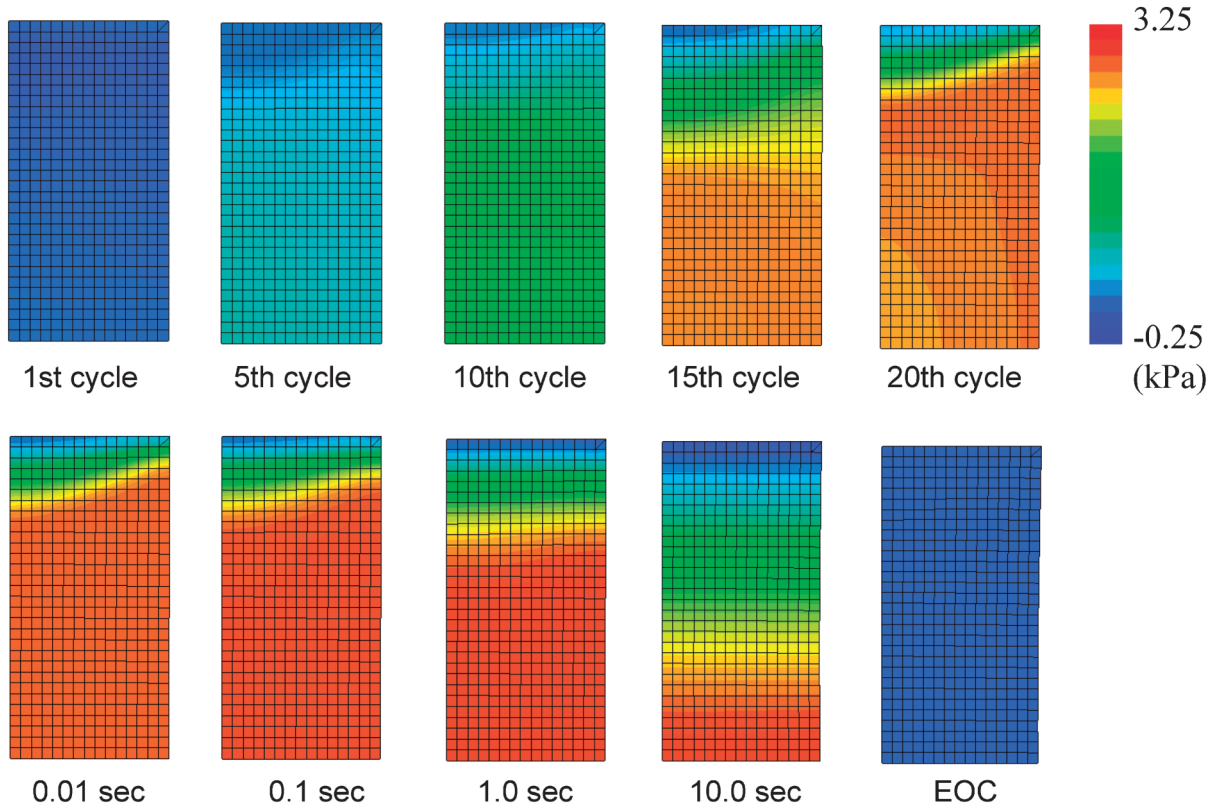

Fig. 13. Distributions of excess pore pressure, u_e with elapsed time (Periods: 0.01 sec)

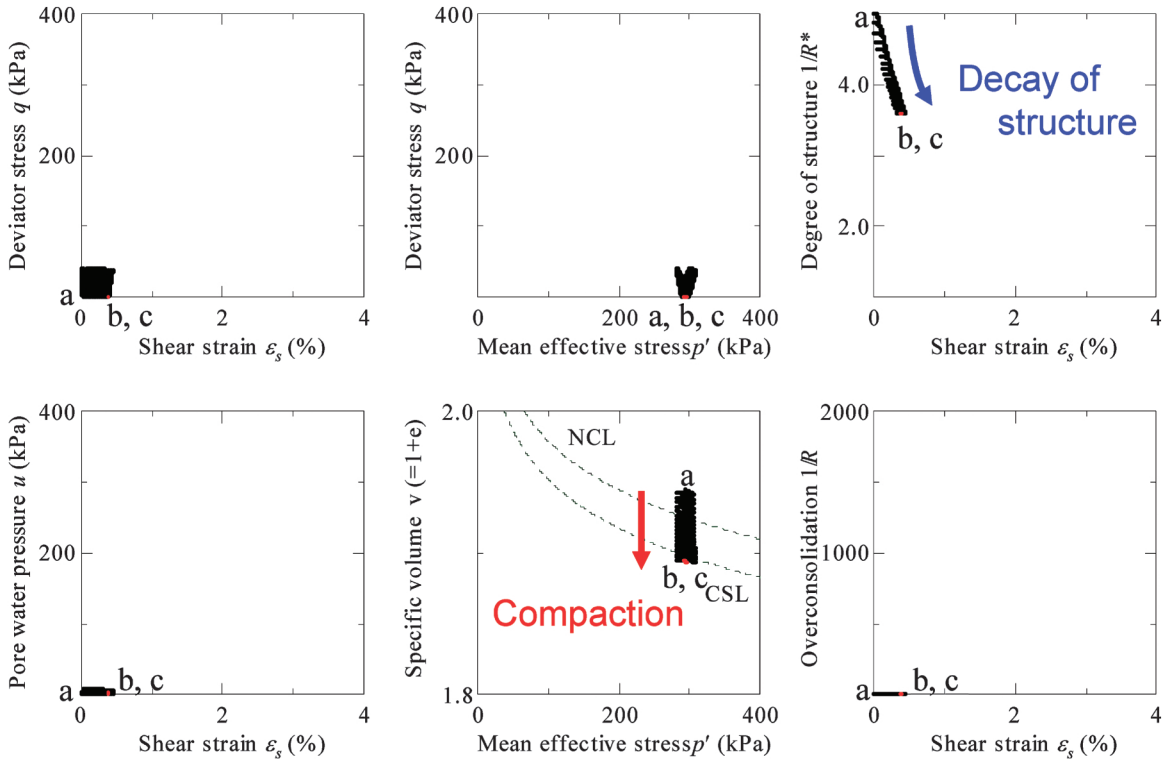

Fig. 14. Compaction behavior of soil element A of Fig. 1 (Periods: 100 sec)

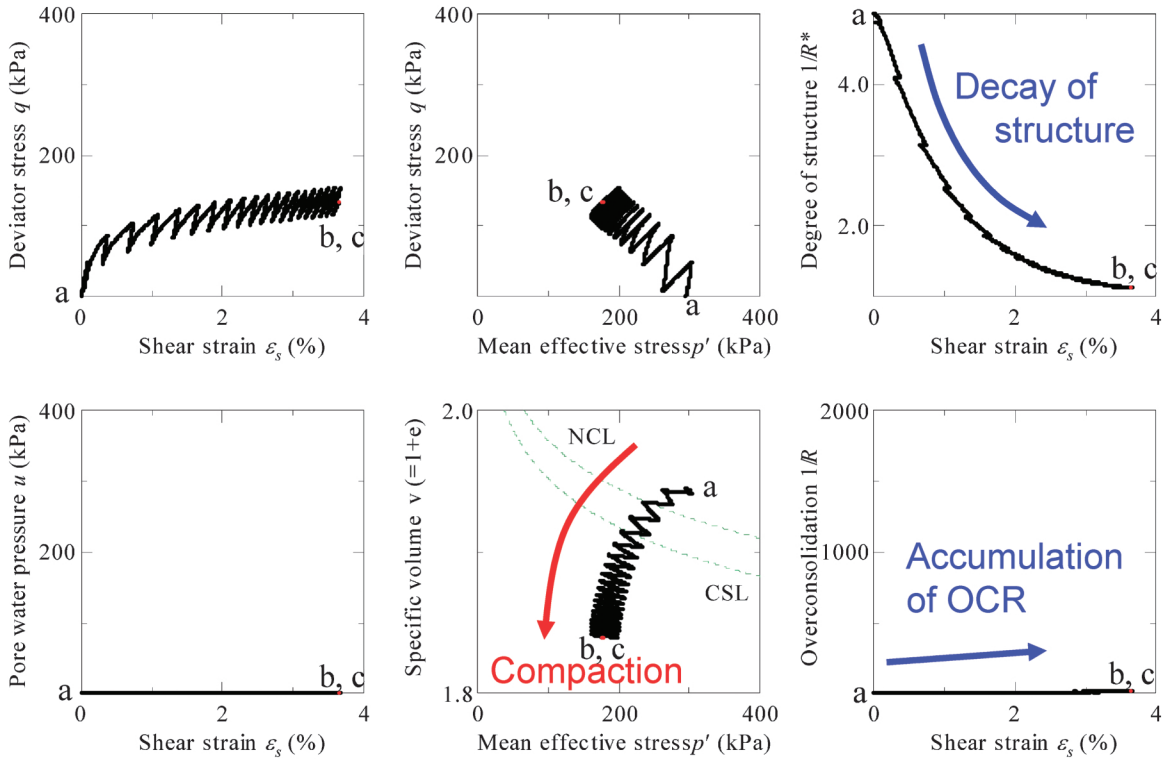

Fig. 15. Compaction behavior of soil element B of Fig. 1 (Periods: 100 sec)

and the amount the compression in it after the end of load application is also small. The above makes it clear that both liquefied areas and compacted areas coexist, even within a single specimen. It is also clear that liquefaction occurs due to the rapid decay of structure and accumulation of overconsolidation caused by the cyclic load and that after liquefaction consolidation, settlement occurs along with relaxation of the accumulated overcon-

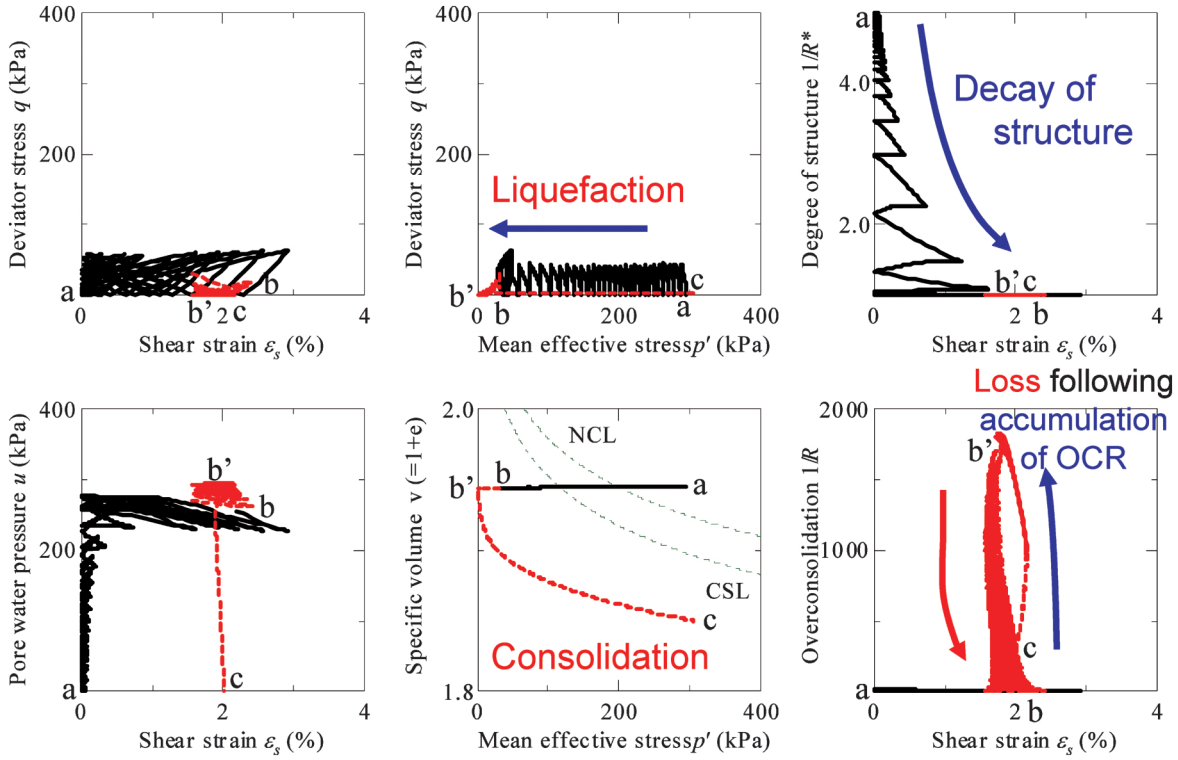

Fig. 16. Liquefaction and liquefaction-induced consolidation behavior of soil element A of Fig. 1 (Periods: 0.01 sec)

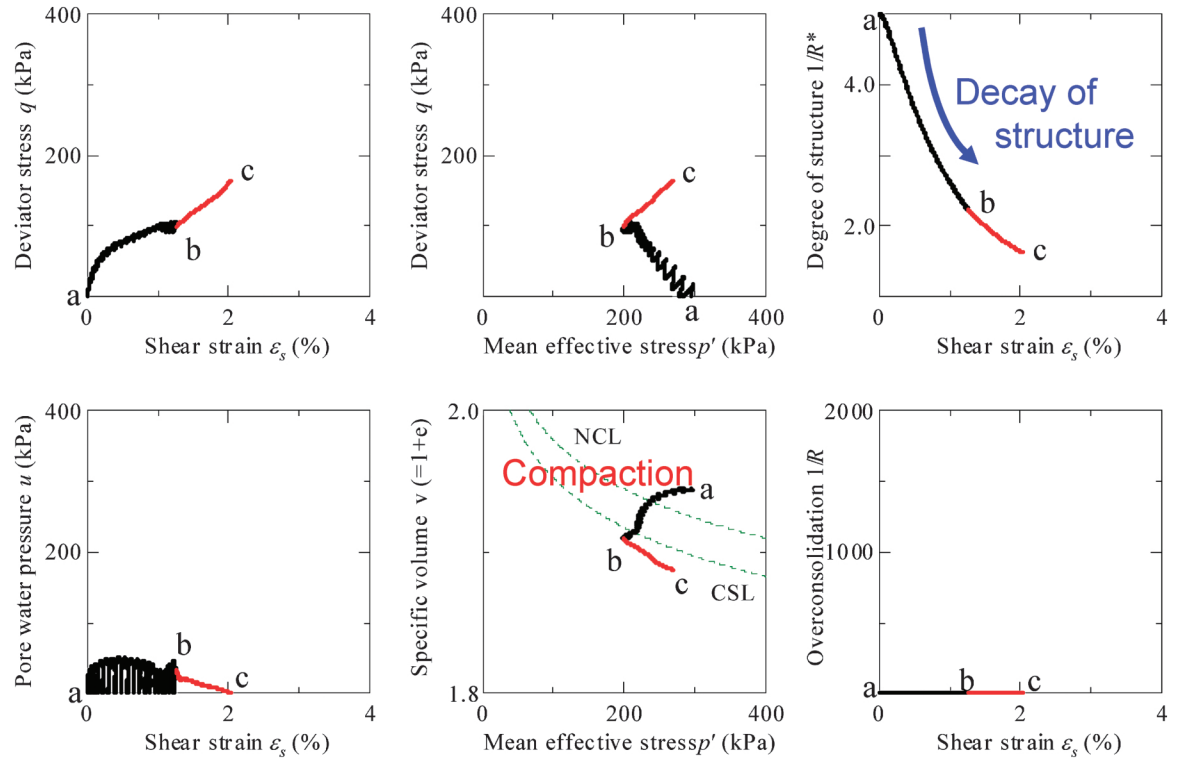

Fig. 17. Consolidation behavior of soil element B of Fig. 1 (Periods: 0.01 sec)

solidation.

Summary of the Calculated Results and Discussion

Under low frequency loading, since the pore water can move sufficiently even during load application, the test specimen exhibits compaction in all regions, with the drained boundary showing the maximum compaction. On the other hand, in the case of high frequencies, liq-

uefaction occurs in deep regions of the specimen during load application, together with compaction at the drained boundary. After load application has ended, compaction and compression progress in those regions where liquefaction had occurred, and the test specimen exhibits massive compression.

In elements such as A (Fig. 17) in deeper parts of the specimen under high frequency loading, why does p' decrease suddenly during and immediately after the end of load application and massive compression occur along with the progress of consolidation? The reason for this can be explained by paying attention to the behavior of the soil skeleton structure (in particular, the decay of structure during loading and the accumulation of overconsolidation during unloading). In other words, we can explain the above phenomenon using the SYS Cam-clay model as follows. When setting the material constants and the initial conditions of the soil in the current calculations, the permeability coefficient assumed was somewhat low, but all other values were typical of medium dense sand (Fig. 2). Compared with typical clay, it can be considered that the soil structure of typical sand decays easily and that loss of overconsolidation is mild (Asaoka et al., 2002; Asaoka, 2003). In terms of the evolutional parameters, this means that compared with clay, a is large and m is small for sand. In addition, since the structures of medium dense and loose sands are in a developed state, repeated stresses arising from the cyclic load cause a rapid decay of structure so that $R^* \to 1$ (APPENDIX 2). Referring to Eq. (A2–1) related to the volume change during loading, it can be seen that decay of structure acts to increase the plastic volume strain $\varepsilon_v^p (= -\int_0^t J\mathrm{tr}\boldsymbol{D}^p d\tau)$ (compression: positive), meaning that plastic compression occurs. Furthermore, since shear under low stresses is produced by the loading pattern, plastic compression is produced during the expansion (i.e., hardening) of the subloading surface as is evident from its shape. On the other hand, since the relaxation of overconsolidation for sand is mild, it is difficult for R to increase towards 1 during loading. Therefore, there is almost no plastic expansion due to loss of overconsolidation, and the plastic compression during load application is much larger than the plastic expansion. This means that in the case of high frequency loading, there is almost no migration of the pore water within the specimen and that element A (Fig. 17) is in a nearly undrained state. Consequently, the elastic and plastic volume strains offset each other ($\dot{\varepsilon}_v^e = -\dot{\varepsilon}_v^p$), and p' corresponding to the elastic volume strain decreases greatly. In addition, since there is residual wave propagation immediately after the end of load application and repeated shear forces continue to act under undrained conditions. As a result, even though the structure was almost lost during loading, expansion of the subloading surface occurs under low stresses (similar to the phenomenon seen during loading), plastic compression is produced, and p' tends to move towards zero (liquefaction). At the same time, since the overconsolidation attained due to repeated shear during unloading is not lost significantly during loading, the overconsolidation ratio continues to increase. In the consolidation stage that follows, for the reason why loss of overconsolidation in the sand is mild, the subloading surface expands while the amount of plastic expansion produced remains small and plastic compression becomes the dominating factor, resulting in massive compression.

Finally, we would like to add that when we compared the above cases of monotonic loading and low frequency loading without the effect of the inertia term with the results of calculations based on the explicit method of analysis not including the inertia term (Asaoka et al., 1994), we found that there was virtually no difference at all between the two cases. Thus, the implicit method of analysis used here can be considered to be a valid method of calculation.

CONCLUSIONS

In this paper, we proposed a new method from the following standpoints in order to deal with inertial forces in the calculation of soil-water coupled finite deformation:

(1) derivation of a rate-type equation of motion for saturated soil containing a jerk term of the soil skeleton conforming to ***u-p*** formulation and updated Lagrangian,
(2) derivation of a weak form of the rate-type equation of motion and finite element discretization, and
(3) application of implicit difference approximation and the Wilson's θ method to the time term. The time term was obtained by applying the linear acceleration method, which assumes linear variation of acceleration, to a jerk term that is one order higher in magnitude than the acceleration term.

The calculations were made by mounting the elastoplastic equation (SYS Cam-clay model), which can be applied to a wide range of soils and soil conditions, onto the above rate-type equation. As an example of application of the derived method of calculation, simulation of dynamic/static triaxial laboratory testing of saturated medium dense sand specimens resembling under conditions of small-amplitude cyclic loading, partial drainage, and constant lateral pressure was carried out. The simulation yielded the following insights:

(1) In the case of low frequencies, compaction occurs during loading and compression progresses over the entire specimen.
(2) In the case of high frequencies, during loading and in the period (0.01 sec in the example here) in which wave propagation continues within the specimen after the end of loading, compaction is produced at the drained end of the specimen, whereas the mean effective stress p' in its interior becomes almost zero. That is to say, liquefaction occurs. This shows that both liquefaction and compaction can coexist within a single specimen. After this stage, massive compression takes place within the specimen, leading to consolidation (consolidation after liquefaction).
(3) The liquefaction and consolidation phenomena described in (2) above are closely related to the events

occurring in the soil skeleton structure of the sand (rapid decay of structure and mild relaxation of overconsolidation). The liquefaction during and immediately after the cessation of loading, is caused by the rapid decay of structure and plastic deformation that accompanies the changes in the subloading surface under low stress ratios. It occurs without relaxation of the accumulating overconsolidation. After this stage, the consolidation deformation that occurs due to the dissipation of the excess pore water pressure is insufficient to release the accumulated overconsolidation soon enough. Because of this, not much plastic expansion is produced, and the occurrence of plastic compression due to expansion of the subloading surface takes precedence.

(4) In the case of high frequency loading, the decay of structure progresses up to the central part of the specimen due to the events described in (3) above, and p' decreases nearly to zero. Thus, even if the number of loading cycles is the same, the specimen is compressed to a greater extent compared with low frequency loading.

(5) For monotonic loading with low loading rates and for low frequency loading, the results of calculation agree almost perfectly with the results obtained by the explicit method of analysis. Thus, the implicit method of analysis used here can be considered to be a valid method of calculation.

REFERENCES

1) Akai, K. and Tamura, T. (1978): Numerical analysis of multi-dimensional consolidation accompanied with elasto-plastic constitutive equation, *Proc. JSCE*, (269), 95–104 (in Japanese).
2) Asaoka, A., Nakano, M. and Noda, T. (1994): Soil-water coupled behaviour of saturated clay near/at critical state, *Soils and Foundations*, **34**(1), 91–106.
3) Asaoka, A., Noda, T. and Fernando, G. S. K. (1997): Effects of changes in geometry on the linear elastic consolidation deformation, *Soils and Foundations*, **37**(1), 29–39.
4) Asaoka, A., Nakano, M. and Noda, T. (1998a): Superloading yield surface concept for the saturated structured soils, *Proc. 4th European Conf. on Numerical Methods in Geotechnical Engineering*, Udine, Italy, 233–242.
5) Asaoka, A., Noda, T. and Kaneda, K. (1998b): 'Displacement/traction boundary conditions represented by constraint conditions on velocity field of soil, *Soils and Foundations*, **38**(4), 173–181.
6) Asaoka, A., Nakano, M. and Noda, T. (2000): Superloading yield surface concept for highly structured soil behavior, *Soils and Foundations*, **40**(2), 99–110.
7) Asaoka, A., Noda, T., Yamada, E., Kaneda, K. and Nakano, M. (2002): An elasto-plastic description of two distinct volume change mechanisms of soils, *Soils and Foundations*, **42**(5), 47–57.
8) Asaoka, A. (2003): Consolidation of clay and compaction of sand–an elastoplastic description, *Proc. 12th Asian Regional Conf. on SMGE (12th ARC)*, Keynote Paper, Singapore, **2**, 1157–1195.
9) Christian, J. T. (1968): Undrained stress distribution by numerical method, *Proc. ASCE*, **94**(SM 6), 1333–1345.
10) de Boer, R.(1998): Theory of porous media–past and present–, *Z. Angew. Math. Mech.*, **78**, 441–446.
11) Green, A. E. and Naghdi, P. M. (1965): A general theory of an elastic-plastic continuum, *Archive for Rational Mechanics and Analysis*, **18**, 251–281.
12) Hashiguchi, K. (1978): Plastic constitutive equations of granular materials, *Proc. US-Japan Seminar on Continuum Mechanics and Statistical Approaches in the Mechanics of Granular Materials* (eds. by Cowin, S. C. and Satake, M.), Sendai, JSSMFE, 321–329.
13) Hashiguchi, K. (1989): Subloading surface model in unconventional plasticity, *International Journal of Solids and Structures*, **25**, 917–945.
14) Li, C., Borja, R. I. and Regueiro, R. A. (2004): Dynamics of porous media at finite strain, *Computational Methods in Applied Mechanics and Engineering*, **193**, 3837–3870.
15) Meroi, E. A., Scherefler, B. A. and Zienkiewicz, O. C. (1995): Large strain static and dynamic semi saturated soil behavior, *International Journal of Numerical and Analytical Methods in Geomechanics*, **19**, 81–106.
16) Nakano, M., Yamada, E. and Noda, T. (2008): Ground improvement of intermediate reclaimed land by compaction through cavity expansion of sand piles, *Soils and Foundations*, **48**(5), 653–671.
17) Nishimura, N. (1999): Chapter 3 Soil Mechanics, *Handbook of Geotechnical Engineering*, The Japanese Geotechnical Society, 51–64 (in Japanese).
18) Noda, T., Asaoka A., Nakano, M., Yamada, E. and Tashiro, M. (2005): Progressive consolidation settlement of naturally deposited clayey soil under embankment loading, *Soils and Foundations*, **45**(5), 39–52.
19) Noda, T., Asaoka, A. and Yamada, S. (2007): Some bearing capacity characteristics of a structured naturally deposited soil, *Soils and Foundations*, **47**(2), 285–301.
20) Oka, F., Yashima, A., Shibata, T. and Kato, M. (1991): A finite element analysis of liquefaction of seabed due to wave action, GEO-COAST '91, 621–626.
21) Oka, F., Yashima, A., Shibata, T., Kato, M. and Uzuoka, R. (1994): FEM-FDM coupled liquefaction analysis of porous soil using an elasto-plastic model, *Applied Scientific Research*, **52**, 209–245.
22) Roscoe, K. H. and Burland, J. B. (1968): On the generalized stress-strain behaviour of 'wet' clay, *Engineering Plasticity* (ed. by Heyman, J. and Leckie, F. A.), Cambridge University Press, 535–609.
23) Schrefler, B. A. (2002): Mechanics and thermodynamics of saturated/unsaturated porous materials and quantitative solutions, *Applied Mechanics Reviews*, ASME, **55**(4), 351–388.
24) Sekiguchi, H. and Ohta, H. (1977): Induced anisotropy and time dependency in clays, *Constitutive Equations of Soils (Proc. 9th ICSMFE, Spec. Session 9)*, Tokyo, Japan, 229–238.
25) Yamada, E. and Nakano, M. (2007): Improvement of manmade island filled with intermediate soils by SCP method, *Proc. 13th Asian Regional Conf. on SMGE (13th ARC)*, Kolkata, India, 787–790.
26) Yatomi, C., Yashima, A., Iizuka, A. and Sano, I. (1989): General theory of shear bands formation by a non-coaxial Cam-clay model, *Soils and Foundations*, **29**(3), 41–53.
27) Wilson, E. L., Farhoomand, I. and Bathe, K.-J. (1973): Nonlinear dynamic analysis of complex structures, *International Journal of Earthquake Engineering and Structural Dynamics*, **1**, 241–252.
28) Zienkiewicz, O. C. and Bettes, P. (1982): Soils and other saturated media under transient, dynamic conditions, *Soils Mechanics-Transient and Cyclic Loads*, New York, John Wiley & Sons, 1–16.
29) Zienkiewicz, O. C. and Shiomi, T. (1984): Dynamic behavior of saturated porous media, The generalized Biot formulation and its numerical solution, *International Journal for Numerical and Analytical Methods in Geomechanics*, **8**(1), 71–96.

APPENDIX 1: APPLICATION OF THE THEORY OF MIXTURES TO THE MECHANICS OF SATURATED SOIL

The theory of mixtures is a mechanical theory used to describe the behavior of a continuum consisting of multiple materials in which the material that fills a given point in space at a given instant is not unique and where the en-

tire system cannot be described by the exclusive motion of a single continuum. The theory has been applied to study the mechanics of saturated soils. Porous media theories based on the continuum theory of mixtures have been extensively developed for many years by numerous researchers, and at present, not only saturated soils but also three-phase systems, unsaturated soils, are being examined. The historical developments and contributions, formulations, etc. in relation to porous media theories have been described in detail by de Boer (1998), Schrefler (2002), and others. Here, in accordance with the descriptive method of Nishimura (1999), we derive the equation of motion with respect to the mechanics of saturated soils and the continuous equations expressing the geometric restrictions between the solid and fluid phases. In the description below, the soil skeleton and pore water, which are the constituent elements of the mixture, will be referred to as the solid phase and fluid phase, respectively. The various quantities with respect to these phases will be represented by the subscripts s and f.

(a) Motion of the solid phase (soil skeleton) and fluid phase (pore water)

The motion of the particles that constitute the solid and fluid phases will be represented by

$$\boldsymbol{x}_s = \boldsymbol{x}_s(\boldsymbol{X}_s,\ t), \quad \boldsymbol{x}_f = \boldsymbol{x}_f(\boldsymbol{X}_f,\ t) \tag{A1-1}$$

where $\boldsymbol{x}_s$ and $\boldsymbol{X}_s$ are the spatial coordinates and the material coordinates, respectively, of the solid phase particles, $\boldsymbol{x}_f$ and $\boldsymbol{X}_f$ are those of the fluid phase particles, and t indicates the time. It is assumed that even though they are different, the relation $\boldsymbol{x}_s(\boldsymbol{X}_s,\ t) = \boldsymbol{x}_f(\boldsymbol{X}_f,\ t)$, can hold for the phases s and f.

(b) Mass conservation law of the solid and fluid phases and the geometric constraints between them

When the true density (after deformation) of the soil particle itself is denoted by ρ^s and that of pore water itself is denoted by ρ^f, *the density* ρ of the mixture is represented by

$$\rho = \sum_a \rho_a, \quad \rho_a = n_a \rho^a, \quad a = (s, f), \tag{A1-2}$$

where ρ_s and ρ_f are the densities of the solid and fluid phases as constituents of the mixture and $n_s = 1 - n$, $n_f = n$. The sum total is not used with respect to phase a as shown in Eq. (A1-2).

By applying the law of mass conservation to phase a,

$$\dot{\rho}_a + \rho_a \operatorname{div} \boldsymbol{v}_a = 0, \tag{A1-3}$$

where the superscript "˙" of a variable is the material time derivative viewed from the phase that is represented by the subscript of the same variable, and $\boldsymbol{v}_a = \dot{\boldsymbol{x}}_a$. Paying attention to the Eulerian form of $\dot{\rho}_a$, addition of Eq. (A1-3) with respect to the solid and fluid phases yields the following.

$$\operatorname{div} \boldsymbol{v}_s + \operatorname{div}\{n(\boldsymbol{v}_f - \boldsymbol{v}_s)\} = -(1-n)\frac{D_s\rho^s}{\rho^s} - n\frac{D_f\rho^f}{\rho^f} \tag{A1-4}$$

(c) Partial and effective stresses in the solid and fluid phases

In terms of the pore water pressure u acting on the saturated soil mixture, the partial stress $\boldsymbol{T}_f$ of the fluid phase is expressed as follows.

$$\boldsymbol{T}_f = -nu\boldsymbol{I} \tag{A1-5}$$

Using the Cauchy stress $\boldsymbol{T}$ or the effective stress $\boldsymbol{T}' = \boldsymbol{T} + u\boldsymbol{I}$, we can obtain the following equation for the partial stress $\boldsymbol{T}_s$ acting on the solid phase.

$$\boldsymbol{T}_s = \boldsymbol{T} - \boldsymbol{T}_f = \boldsymbol{T} + nu\boldsymbol{I} = \boldsymbol{T}' - (1-n)u\boldsymbol{I} \tag{A1-6}$$

That is to say, in the mechanics of saturated soils in general, the effective stress that is effective for deforming the soil skeleton is not the partial stress that acts on the soil skeleton. Furthermore, the partial stresses $\boldsymbol{T}_f$ and $\boldsymbol{T}_s$ exhibit symmetry as will be shown later in Eq. (A1-7)[2].

(d) Equations of motion and the Darcy Law

From the laws of conservation of the amount of motion and the amount of angular motion of each phase and the law of conservation of mass [Eq. (A1-4)], the equation for phase a becomes

$$\rho_a \ddot{\boldsymbol{x}}_a = \operatorname{div} \boldsymbol{T}_a + \rho_a \boldsymbol{b} + \boldsymbol{I}_a, \quad \boldsymbol{T}_a^{\mathrm{T}} = \boldsymbol{T}_a \tag{A1-7}$$

where $\boldsymbol{b}$ is the body for per unit mass and $\boldsymbol{I}_a$ expresses the mutual interactions of the other phases on phase a. From the law of action and reaction, the equation $\Sigma_a \boldsymbol{I}_a = \boldsymbol{0}$ must be satisfied. It is assumed here that there are no interaction couples. For the case, $\boldsymbol{I}_s = -\boldsymbol{I}_f$, we follow the example of de Boer (1998) and Nishimura (1999). From the analogy to the Hagen-Poiseuille solution of the problem of steady viscous flow within a uniform cylinder of infinite length to obtain the forces acting within the cylinder, the following equation is derived by additional consideration of the effect of porosity gradient.

$$\boldsymbol{I}_f = -\boldsymbol{I}_s = -\gamma_w n^2 \boldsymbol{K}^{-1}(\boldsymbol{v}_f - \boldsymbol{v}_s) + u \operatorname{grad} n \tag{A1-8}$$

Here, $\boldsymbol{K}$ is an objective tensor of the 2nd order called the permeability coefficient tensor. In the case of isotropy, $\boldsymbol{K} = k\boldsymbol{I}$, and k is called the coefficient of permeability. In the case when the acceleration term can be ignored, Eq. (A1-7)[1] with respect to f matches the Darcy Law. From the principle of objectivity, $\boldsymbol{K}$ will be a constant only in the case of isotropy. Furthermore, when we take the sum with respect to a in Eq. (A1-7)[1], the equation for the external force acting on saturated soil is obtained as follows.

$$\rho_s \ddot{\boldsymbol{x}}_s + \rho_f \ddot{\boldsymbol{x}}_f = \operatorname{div} \boldsymbol{T} + \rho \boldsymbol{b} \tag{A1-9}$$

Here, assuming the soil particles and pore water to be incompressible, let us consider the equations defining the density of each phase (Eq. (A1-2): No. of equations = 2), the equations based on the mass conservation law (Eq. (A1-5): No. of equations = 2), the equations of motion (Eq. (A1-7): No. of equations = 6), and the constitutive equation of the soil skeleton. If we substitute the constitutive equation of the soil skeleton in Eq. (A1-9), the number of equations becomes 10. The unknowns are displacement components of the solid and fluid phases (3

unknowns each), pore water pressure u, ρ_s, ρ_f, and the pore ratio n. The total of unknowns is therefore 10, and we have a closed system of equations. In the actual solution of the problem of saturated soils (mixtures), we can substitute Eq. (A1–2)[2] suitably in other equations in order to determine the pore water pressure u and each of the three displacement components (or spatial coordinates) of the solid and fluid phases (i.e., a total of 7 unknowns) through the system of 7 simultaneous equations consisting of Eq. (A1–4), Eq. (A1–7) with respect to the fluid, and Eq. (A1–9). This is called Full formulation.

APPENDIX 2: THE SUPER/SUBLOADING YIELD SURFACE (SYS) CAM-CLAY MODEL

The Quantified Expression of Structure, Overconsolidation, Anisotropy, and Their Respective Evolution Rules

Naturally deposited soils, whether clayey or sandy, generally exist in a 'structured' and overconsolidated state. To describe the deformation behavior of a soil in this state, we have to start from the base of an elasto-plastic model of a de-structured soil in a state of normal consolidation. Given that a soil in this unstructured and normally consolidated state still possesses anisotropy, we take for our 'base' in this paper the Modified Cam-clay model (Roscoe and Burland (1968)) with the introduced addition of the rotational hardening concept of Sekiguchi and Ohta (1977), which treats stress parameter η^* and its evolution rule as an expression of anisotropy. The degrees of structure and overconsolidation are then introduced and quantified by means of the two concepts of the superloading surface for structure (Asaoka et al., 1998a, 2000, 2002), and the subloading surface for overconsolidation (Hashiguchi, 1978, 1989; Asaoka et al., 1997). That is to say, the degree of structure is expressed by means of a superloading surface situated on the outside of the Cam-clay normal-yield surface and similar to it (the center of similarity being the origin $p'=q=0$ and the similarity rate being given by R^* $(0<R^*\leq 1)$, while the overconsolidation state is expressed by means of a subloading surface situated on the inside of the superloading surface and again similar to it (center of similarity $p'=q=0$, similarity rate R $(0<R\leq 1)$); reciprocal $1/R$ is the overconsolidation ratio). The closer R^* is to 0 the higher the degree of structure, but with the loss of structure that accompanies progressive plastic deformation R^* will approach 1 (evolution rule for R^*). Similarly, the closer R is to 0 the more overconsolidated the state of the soil, but as R increases toward 1 with plastic deformation, the state of the soil will also approach normal consolidation (evolution rule for R). It can thus be assumed that the decay of structure with progressive plastic deformation brings a simultaneous loss from overconsolidation (a transition to the normally consolidated state), resulting finally in conditions that match those in the Cam-clay model. The relative positions of the three loading surfaces, assuming conditions of axial symmetry, are as shown in Fig. A2–1.

If we start from the Modified Cam-clay as our base,

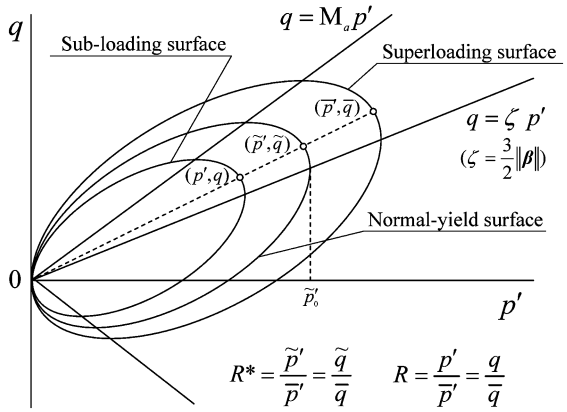

Fig. A2–1. Three loading surfaces

given that the current effective stress exists on the subloading surface shown below, we need to adapt relations to the subloading surface through the application of various elasto-plastic principles such as the associated flow rule and Prager's consistency condition.

The subloading surface:

$$\mathrm{MD}\ln\frac{p'}{\tilde{p}'_0}+\mathrm{MD}\ln\frac{\mathrm{M}^2+\eta^{*2}}{\mathrm{M}^2}+\mathrm{MD}\ln R^*-\mathrm{MD}\ln R+\int_0^t J\mathrm{tr}\boldsymbol{D}^p d\tau=f(p',\eta^*)+\mathrm{MD}\ln\frac{R^*}{R}+\int_0^t J\mathrm{tr}\boldsymbol{D}^p d\tau=0 \quad \text{(A2–1)}$$

Here, $\mathrm{D}=(\tilde{\lambda}-\tilde{\kappa})/\mathrm{M}/(1+\mathrm{e}_0)$ is the dilatancy coefficient, and M, $\tilde{\lambda}$, $\tilde{\kappa}$ and e_0 are the critical state constant, compression index, swelling index, and initial void ratio. $J=(1+\mathrm{e})/(1+\mathrm{e}_0)$ (e is the void ratio at time $t=t$). $-\int_0^t J\mathrm{tr}\boldsymbol{D}^p d\tau$ corresponds to the plastic volumetric strain η^*, the expression of anisotropy, is obtained using the rotational hardening variable $\boldsymbol{\beta}$, from the calculation $\eta^*=\sqrt{3/2}\hat{\boldsymbol{\eta}}\cdot\hat{\boldsymbol{\eta}}$, $\hat{\boldsymbol{\eta}}=\boldsymbol{\eta}-\boldsymbol{\beta}$, $\boldsymbol{\eta}=\boldsymbol{S}/p'$. $\boldsymbol{\beta}=\boldsymbol{0}$ expresses a state of no anisotropy. In the present paper, the evolution rules for R^*, R and $\boldsymbol{\beta}$ are given by the following equations.

$$\dot{R}^*=J\sqrt{\frac{2}{3}}\|\boldsymbol{D}^p_s\|,\quad U^*=\frac{a}{\mathrm{D}}R^{*b}(1-R^*)^c \quad \text{(A2–2)}$$

$$\dot{R}=JU\|\boldsymbol{D}^p\|,\quad U=-\frac{m}{\mathrm{D}}\ln R \quad \text{(A2–3)}$$

$$\mathring{\boldsymbol{\beta}}=J\frac{br}{\mathrm{D}}\sqrt{\frac{2}{3}}\|\boldsymbol{D}^p_s\|\ \|\hat{\boldsymbol{\eta}}\|\left(m_b\frac{\hat{\boldsymbol{\eta}}}{\|\hat{\boldsymbol{\eta}}\|}-\boldsymbol{\beta}\right), \quad \text{(A2–4)}$$

where $\boldsymbol{D}^p$ is the plastic stretching tensor, $\boldsymbol{D}^p_s$ is the deviator component of $\boldsymbol{D}^p$ and $\|\ \|$ represents its Euclidian norm. $\mathring{\boldsymbol{\beta}}$ in Eq. (A2–4) is the Green-Nahdhi's (1965) rate of $\boldsymbol{\beta}$. The parameter groups for the evolution rules in Eqs. (A2–2)–(A2–4) all consists of constants, and from their respective functions we may call a, b, c the degradation indices of structure, m the degradation index of overconsolidation, br the rotational hardening index, and m_b the rotational hardening limit constant.

APPENDIX 3: CONCRETE FORMS OF THE MATRICES AND VECTORS

The displacement velocity $\boldsymbol{v}^e$ of any given point within an element is approximated by the following equation using the shape factor N^k and displacement velocity $\boldsymbol{v}_k^e$ of each node of the element ($k=1, 2, \cdots, p$; p is the number of nodes of the element. In the case of plane strain or axisymmetric conditions, $p=4$; $p=8$ under three-dimensional conditions).

$$\boldsymbol{v}^e = N^k \boldsymbol{v}_k^e \tag{A3-1}$$

By using the symbols { } and [ ] to express the column and matrix vectors, respectively, of the tensor and vector quantity components, we obtain the following equations.

$$\{\boldsymbol{v}^e\} = [N]\{\boldsymbol{v}^i\} \tag{A3-2}$$

$$\{\boldsymbol{D}\} = [B]\{\boldsymbol{v}^i\} \tag{A3-3}$$

$$\{\boldsymbol{L}\} = [M]\{\boldsymbol{v}^i\} \tag{A3-4}$$

$$\mathrm{tr}\ \boldsymbol{D} = [B_v]\{\boldsymbol{v}^i\} \tag{A3-5}$$

$$\{\boldsymbol{v}^i\} = \{\boldsymbol{v}_1^{e\mathrm{T}}\ \ \boldsymbol{v}_2^{e\mathrm{T}} \cdots \boldsymbol{v}_{(p-1)}^{e\mathrm{T}}\ \ \boldsymbol{v}_p^{e\mathrm{T}}\}^{\mathrm{T}} \tag{A3-6}$$

When the geometric quantities within the element are expressed by the above, M^i, K^i, L^i, and $\{\dot{\boldsymbol{f}}^i\}$ of Eq. (22) are expressed by the following equations.

$$\mathrm{M}^i = \int_v \rho [N]^{\mathrm{T}}[N]dv \tag{A3-7}$$

$$\mathrm{K}^i = \int_v [B]^{\mathrm{T}}[D^{ep}][B]dv + \int_v [M]^{\mathrm{T}}[T_1][M]dv + \int_v \rho^f [N]^{\mathrm{T}}([N]\{\dot{\boldsymbol{v}}^i\} - \{\boldsymbol{b}\})[B_v]dv \tag{A3-8}$$

$$\mathrm{L}^i = \int_v [B_v]dv \tag{A3-9}$$

$$\mathrm{L}_{\mathrm{c}}^i = -\int_v \rho^f \frac{n}{K_f}[N]^{\mathrm{T}}([N]\{\dot{\boldsymbol{v}}^i\} - \{\boldsymbol{b}\})dv \tag{A3-10}$$

$$\{\dot{\boldsymbol{f}}^i\} = \int_a [N]^{\mathrm{T}}\{\dot{\boldsymbol{s}}_t\}da - \int_v [B]^{\mathrm{T}}\{T'_\Omega\}dv \tag{A3-11}$$

In Eq. (A3-8) above, $[\boldsymbol{D}^{ep}]$ is the elasto-plastic matrix and $[T_1]$ is the matrix obtained from $(\mathrm{tr}\boldsymbol{D})\boldsymbol{T}\cdot\delta\boldsymbol{L} - \boldsymbol{T}\boldsymbol{L}^{\mathrm{T}}\cdot\delta\boldsymbol{L}$ in Eq. (16). The first term on the right-hand side of Eq. (A3-11) is the equivalent traction rate vector of element i obtained from Eq. (14). $\{T'_\Omega\}$ is the column vector obtained from $(\boldsymbol{\Omega}\boldsymbol{T}' - \boldsymbol{T}'\boldsymbol{\Omega})\cdot\delta\boldsymbol{D}$, which is the second term on the right-hand side of Eq. (16).

APPENDIX 4: PHYSICAL MODEL OF THE SOIL SKELETON - PORE WATER COUPLED EQUATION

H^i in Eq. (26) is given by

$$\mathrm{H}^i = \left[\alpha_1^i \cdots \alpha_m^i \cdots \alpha_s^i\ -\sum_{m=1}^{s}\alpha_m^i\right], \tag{A4-1}$$

where α_m^i of the soil skeleton–pore water coupled equation (Eq. (18)) is expressed as follows in the case of inhomogeneity (Fig. A4-1).

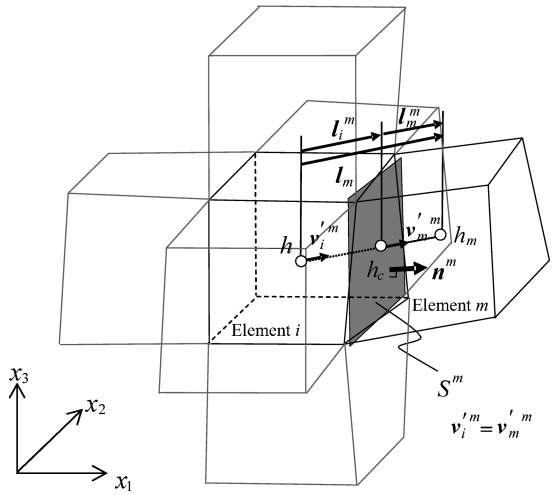

Fig. A4-1. Physical model of pore water flow (in the three-dimensional case)

$$\alpha_m^i = \frac{k_i k_m}{k_i l_m^m + k_m l_i^m}\frac{\boldsymbol{l}^m\cdot\boldsymbol{n}^m}{l^m}S^m \quad \text{(No sum)} \tag{A4-2}$$

Here, k_i is the coefficient of permeability of element i, k_m is the coefficient of permeability of element m, $\boldsymbol{v}_i'^m$ is the (relative) flow rate vector of pore water in element i moving toward element m, $\boldsymbol{v}_m'^m$ is the (relative) flow rate vector of pore water in element m moving in from element i, $\boldsymbol{n}^m$ is the outward bound unit normal vector (viewed from element i) perpendicular to the surface formed by the two vectors that connect the two groups of two nodes lying facing one another on the boundary surface between elements i and m, S^m is the area of the boundary surface between elements i and m when it is projected on the surface that contains the unit normal vector $\boldsymbol{n}^m$ and passes through the center of gravity of the above boundary surface (between elements i and m), $\boldsymbol{l}_i^m$ is the relative positional vector directed toward the center of gravity of the boundary surface between elements i and m, viewed from the center of gravity of element i, $\boldsymbol{l}_m^m$ is the relative positional vector directed toward the center of gravity of element m, viewed from the center of gravity of the boundary surface between elements i and m, l_i^m is the Euclidian norm of $\boldsymbol{l}_i^m$, l_m^m is the Euclidian norm of $\boldsymbol{l}_m^m$, and s is the number of adjacent finite elements. In the three-dimensional case, $s=6$, and under two-dimensional plane strain or axisymmetric conditions, $s=4$.

Figure A4-1 is a physical model of pore water flow for the three-dimensional case. Eq. (A4-2) can be used even for two-dimensional plane strain conditions. In such a case, however, $\boldsymbol{n}^i$ is the outward bound unit normal vector that is perpendicular to the edge common to elements A and i. S^i is equivalent to the length of the common edge. In the case of axisymmetric conditions, it is necessary, in addition to modeling as for two-dimensional plane strain case, to take into consideration in Eq. (A4-2) the distance between the axis of rotational symmetry and the center of the element or edge (Asaoka et al., 1994, 1997).